

# The Changing Biological Carbon Pump of the South Atlantic Ocean

Louise Delaigue<sup>1</sup>, Olivier Sulpis<sup>2</sup>, Gert-Jan Reichart<sup>3</sup>, and Matthew Paul Humphreys<sup>4</sup>

<sup>1</sup>NIOZ Royal Netherlands Institute for Sea Research

<sup>2</sup>CEREGE

<sup>3</sup>NIOZ

<sup>4</sup>Royal Netherlands Institute for Sea Research

April 15, 2024

## Abstract

Global marine anthropogenic CO<sub>2</sub> inventories have traditionally emphasized the North Atlantic's role in the carbon cycle, while Southern hemisphere processes are less understood. The South Subtropical Convergence (SSTC) in the South Atlantic, a juncture of distinct nutrient-rich waters, offers a valuable study area for discerning the potential impacts of climate change on the ocean's biological carbon pump (C<sub>soft</sub>). Using discrete observations from GLODAPv2.2022 and BGC-Argo at 40°S in the Atlantic Ocean, an increase in dissolved inorganic carbon (DIC) of  $+1.44 \pm 0.11 \mu\text{mol kg}^{-1} \text{ yr}^{-1}$  in surface waters was observed. While anthropogenic CO<sub>2</sub> played a role, variations in the contribution of C<sub>soft</sub> were observed. Discrepancies emerged in assessing C<sub>soft</sub> based on the tracers employed: when using AOU, C<sub>soft</sub>(AOU) recorded an increase of  $+0.20 \pm 0.03 \mu\text{mol kg}^{-1} \text{ yr}^{-1}$ , whereas, using nitrate as the reference, C<sub>soft</sub>(NO<sub>3</sub>) displayed an increase of  $+0.85 \pm 0.07 \mu\text{mol kg}^{-1} \text{ yr}^{-1}$ . Nonetheless, our observations at 40°S indicate a significant intensification of C<sub>soft</sub>, which, scaled to the entire ocean, represents an additional 23% to 35% of organic carbon degradation within the water column. Key processes such as water mass composition shifts, changes in oxygenation, remineralization in the Southern Ocean, and the challenges they pose in accurately representing the evolving C<sub>soft</sub> are discussed. These findings highlight that while global studies primarily attribute DIC increase to anthropogenic CO<sub>2</sub>, observations at 40°S reveal an intensified biological carbon pump, showing that regional DIC changes are more complex than previously thought and challenging the dominance of anthropogenic sources in global DIC change.

## Hosted file

Delaigue\_SA\_manuscript\_v18.docx available at <https://authorea.com/users/768752/articles/833767-the-changing-biological-carbon-pump-of-the-south-atlantic-ocean>

## Hosted file

Delaigue\_SA\_supp\_v2.docx available at <https://authorea.com/users/768752/articles/833767-the-changing-biological-carbon-pump-of-the-south-atlantic-ocean>

1 **The Changing Biological Carbon Pump of the South Atlantic Ocean**  
2 **L. Delaigue<sup>1\*</sup>, O. Sulpis<sup>2,3</sup>, G-J Reichart<sup>1,3</sup> and M. P. Humphreys<sup>1</sup>**

3 <sup>1</sup>Department of Ocean Systems (OCS), NIOZ Royal Netherlands Institute for Sea Research, PO  
4 Box 59, 1790 AB Den Burg (Texel), the Netherlands

5 <sup>2</sup>CEREGE, Aix Marseille Univ, CNRS, IRD, INRAE, Collège de France, Aix-en-Provence,  
6 France

7 <sup>3</sup>Department of Earth Sciences, Utrecht University, Utrecht, the Netherlands.

8  
9  
10 \*Corresponding author: Louise Delaigue ([louise.delaigue@nioz.nl](mailto:louise.delaigue@nioz.nl))  
11

12 **Key Points:**

- 13 • The South Subtropical Convergence (SSTC) at 40°S in the Atlantic Ocean shows an  
14 intensified biological carbon pump, amidst uncertainties.
- 15 • Uncertainties stem from local and far-field physical and biological changes impacting  
16 remineralization processes that are reflected at 40°S.
- 17 • Scaled to the entire ocean, this intensification marks an extra 23-35% of organic carbon  
18 degradation, challenging usual CO<sub>2</sub> inventory focus.

19  
20 **Abstract**

21 Global marine anthropogenic CO<sub>2</sub> inventories have traditionally emphasized the North Atlantic's  
22 role in the carbon cycle, while Southern hemisphere processes are less understood. The South  
23 Subtropical Convergence (SSTC) in the South Atlantic, a juncture of distinct nutrient-rich  
24 waters, offers a valuable study area for discerning the potential impacts of climate change on the  
25 ocean's biological carbon pump (C<sub>soft</sub>). Using discrete observations from GLODAPv2.2022 and  
26 BGC-Argo at 40°S in the Atlantic Ocean, an increase in dissolved inorganic carbon (DIC) of  
27  $+1.44 \pm 0.11 \mu\text{mol kg}^{-1} \text{yr}^{-1}$  in surface waters was observed. While anthropogenic CO<sub>2</sub> played a  
28 role, variations in the contribution of C<sub>soft</sub> were observed. Discrepancies emerged in assessing  
29 C<sub>soft</sub> based on the tracers employed: when using AOU, C<sub>soft(AOU)</sub> recorded an increase of  $+0.20 \pm$   
30  $0.03 \mu\text{mol kg}^{-1} \text{yr}^{-1}$ , whereas, using nitrate as the reference, C<sub>soft(NO<sub>3</sub>)</sub> displayed an increase of  
31  $+0.85 \pm 0.07 \mu\text{mol kg}^{-1} \text{yr}^{-1}$ . Nonetheless, our observations at 40°S indicate a significant  
32 intensification of C<sub>soft</sub>, which, scaled to the entire ocean, represents an additional 23% to 35% of  
33 organic carbon degradation within the water column. Key processes such as water mass  
34 composition shifts, changes in oxygenation, remineralization in the Southern Ocean, and the  
35 challenges they pose in accurately representing the evolving C<sub>soft</sub> are discussed. These findings  
36 highlight that while global studies primarily attribute DIC increase to anthropogenic CO<sub>2</sub>,  
37 observations at 40°S reveal an intensified biological carbon pump, showing that regional DIC  
38 changes are more complex than previously thought and challenging the dominance of  
39 anthropogenic sources in global DIC change.  
40

## 41 **Plain language summary**

42 The South Atlantic Ocean at 40°S has experienced changes in dissolved inorganic carbon (DIC)  
43 levels over the years, affecting its carbon composition. This study running from 1972 to 2023  
44 showcased an increase in DIC down to 2,000 meters deep. While anthropogenic CO<sub>2</sub> has  
45 traditionally been seen as the major contributor, the biological carbon pump's activity, influenced  
46 by various ocean processes, emerged as a significant driver. Specifically, factors such as  
47 photosynthesis, organic matter remineralization, sea ice movements, and freshwater influx from  
48 melting ice play pivotal roles in dictating oxygen and nitrate levels, both crucial components to  
49 predict the biological carbon pump's contribution to DIC. Our findings emphasize that this  
50 enhanced biological pump might contribute as much as human-made CO<sub>2</sub> to DIC in certain  
51 ocean regions. If unchecked, these changes could recalibrate ocean carbon budgets and  
52 predictions, with potential shifts in water mass compositions, demanding more vigilant future  
53 monitoring.

## 54 **1 Introduction**

55 The ocean has been acting as a sink for anthropogenic CO<sub>2</sub>, absorbing an estimated 24% of  
56 anthropogenic CO<sub>2</sub> since the beginning of the industrial era, thus significantly mitigating climate  
57 change (Friedlingstein et al., 2023; Gruber et al., 2023). Part of this anthropogenic carbon  
58 remains in the form of dissolved inorganic carbon (DIC) and is transported into the ocean  
59 interior (Davila et al., 2022; Gruber et al., 2019; Khatiwala et al., 2009; Sabine & Tanhua, 2010;  
60 Sarmiento et al., 1992), and part of it is incorporated by marine organisms into organic matter or  
61 calcium carbonate (Heinze et al., 1991; Sarmiento et al., 1998; Volk & Hoffert, 1985).

62 The sequence of processes that store atmospheric carbon as biogenic matter at the surface ocean  
63 and sequester a small fraction of it in deep-sea sediments, where it can be stored permanently, is  
64 named the “biological pump” (Riebesell et al., 2009). While recent studies have focused on  
65 quantifying anthropogenic CO<sub>2</sub> uptake by the ocean at the air-sea interface, or its fate into the  
66 ocean interior as DIC, little is known about its effect on and removal by the biological carbon  
67 pump (BCP) over recent years, despite its importance for understanding future ocean carbon  
68 cycling. Biological processes in the upper ocean annually convert approximately 50-60 gigatons  
69 of dissolved inorganic carbon into organic matter (De La Rocha & Passow, 2014). Out of this  
70 amount, around 10% is transported out of the surface ocean in the form of organic carbon (De La  
71 Rocha & Passow, 2014). Through this natural and anthropogenic carbon export, the BCP lowers  
72 atmospheric CO<sub>2</sub> levels by ~200 ppm relative to a world without it (Henson et al., 2022). It is  
73 thus essential that we understand the drivers and variability of the BCP and its vulnerability to  
74 current anthropogenic changes to predict future climate. However, the complexity of ecosystem  
75 functioning and composition makes estimates of both present-day and future organic carbon  
76 export poorly constrained, in models and observations (Henson et al., 2022; Henson et al., 2012;  
77 Laufkötter et al., 2016; Marsay et al., 2015).

78 The oceanic distribution of DIC is mainly controlled by three pumps: the biological processes of  
79 photosynthesis, respiration, and remineralization (i.e. the soft-tissue pump, C<sub>soft</sub>), the formation  
80 and dissolution of calcium carbonate (i.e. the carbonate pump, C<sub>carb</sub>) and the uptake of natural  
81 and anthropogenic CO<sub>2</sub> (i.e. the solubility pump, C<sub>anth</sub>; Gruber et al., 1996; Volk & Hoffert,  
82 1985). While the solubility pump accounts for 30-40% of ocean carbon export flux to the deep  
83 ocean (Gruber et al., 2002; Toggweiler et al., 2003), the remaining portion is transported from  
84 the sunlit surface to the deep ocean as photosynthetically fixed organic carbon by the soft tissue

85 pump (Riebesell et al., 2009; Schlunegger et al., 2019). To quantify the rate of soft tissue and  
86 carbonate pump changes, one could monitor particulate organic and inorganic carbon sinking  
87 fluxes through time, but sediment trap data are sparse and associated with large uncertainties  
88 (Buesseler et al., 2007). Monitoring changes in DIC is also complicated because  $C_{soft}$ ,  $C_{carb}$ , and  
89  $C_{anth}$  cannot be readily distinguished from the DIC analyses themselves. Instead, one can unravel  
90 the different components of the carbon pump and changes therein by combining multiple  
91 proxies, such as the apparent oxygen utilization (AOU; the difference between the saturation  
92 oxygen concentration,  $[O_{2,sat}]$  and the observed oxygen concentration,  $[O_2]$ ), or release rates of  
93 organic-matter degradation byproducts, i.e.,  $NO_3$ ,  $PO_4$  or alkalinity. For the carbonate pump,  
94 calcification and dissolution can be tracked in seawater by measuring dissolved calcium or  
95 alkalinity changes (Chen, 1978; Feely et al., 2004). Carbon sequestration by the soft tissue pump  
96 can be estimated from nutrient and oxygen observations, taking advantage of the constant  
97 stoichiometric ratios of carbon, nutrients, and oxygen in marine organic matter in the open  
98 ocean, also known as the Redfield Ratio (Ito & Follows, 2005; Redfield, 1958). Using the latter,  
99 these variables are converted back to carbon units in the natural components of DIC ( $C_{carb}$ , and  
100  $C_{soft}$ ) as well as anthropogenic  $CO_2$  ( $C_{anth}$ ), allowing for the disentanglement of changes in each  
101 DIC component.

102  
103 Although global evaluations of the oceanic  $CO_2$  inventory have often highlighted the North  
104 Atlantic Ocean as the primary region of interest for anthropogenic  $CO_2$  subduction, with a  
105 storage estimated at 23% of global ocean anthropogenic  $CO_2$  (Khatiwala et al., 2013; Sabine et  
106 al., 2004), the importance of southern hemisphere processes, such as the formation of Antarctic  
107 Intermediate Water (AAIW), has recently gained attention (Groeskamp et al., 2016;  
108 Landschützer et al., 2015). The South Subtropical Convergence (SSTC), an intersection point of  
109 low-macronutrient subtropical gyre waters and high-macronutrient Antarctic Circumpolar  
110 Current waters, is a significant biogeochemical feature of the South Atlantic Ocean (Browning et  
111 al., 2014). This convergence zone results in strong downwelling and pronounced surface  
112 gradients in salinity and temperature, leading to distinct water column stratification with shallow  
113 mixing in a thermally homogeneous surface layer, increasing light availability and productivity  
114 (Browning et al., 2014). Such stratification can impact the marine carbon cycle by potentially  
115 inhibiting the transport of heat, oxygen, and carbon dioxide deeper into the ocean (Li et al.,  
116 2020).

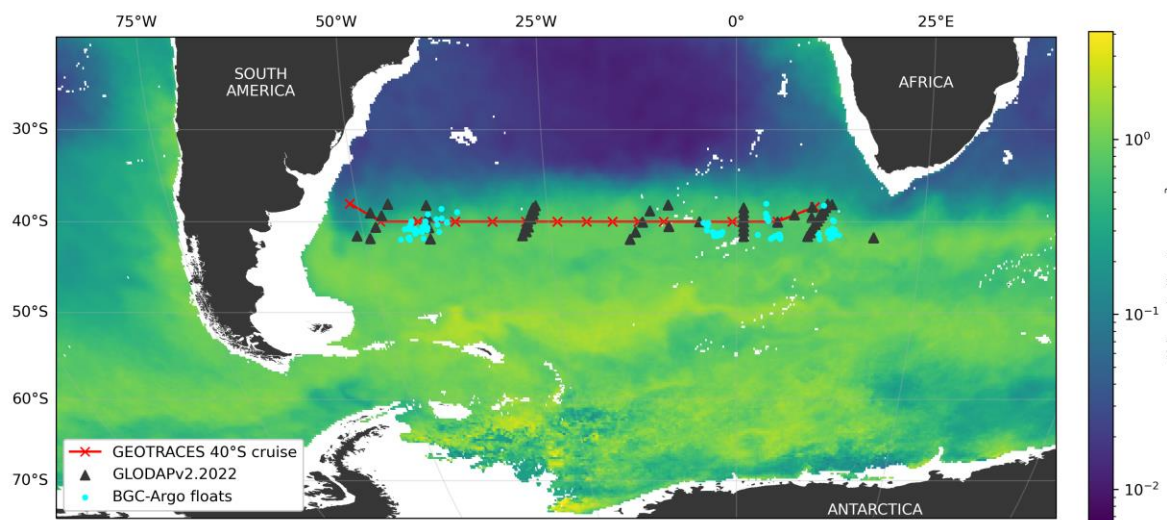
117  
118 Simultaneously, the Southern Ocean is known for its high macronutrient supply, primarily from  
119 the upwelling of nutrient-rich deep waters (Moore et al., 2001; Tagliabue et al., 2014). These  
120 waters provide nitrate that fuels primary production. As organic matter produced in the Southern  
121 Ocean sinks to the SSTC region, it undergoes remineralization, converting back into inorganic  
122 nutrients. Nitrate concentrations can thus indicate the extent of remineralization in an area  
123 (Moore et al., 2001; Tagliabue et al., 2014), with higher concentrations suggesting more organic  
124 matter has been remineralized. This enhanced remineralization, fueled by the increased nitrate  
125 supply from Southern Ocean waters, may then contribute to a stronger soft tissue pump and  
126 carbon export to deeper waters (Boyd & Trull, 2007; Sarmiento, 2006)

127  
128 Although not historically prominent, anticipated changes in the BCP are emerging due to specific  
129 climatic and oceanographic drivers. Behrenfeld et al. (2006) reported alterations in ocean  
130 productivity linked to climate change, with increased stratification in some regions affecting

131 primary production. Polovina et al. (2008) identified the expansion of subtropical gyres and  
132 associated shifts in phytoplankton communities in the Pacific. Furthermore, Orr et al. (2005)  
133 demonstrated that escalating CO<sub>2</sub> concentrations lead to ocean acidification, challenging marine  
134 calcifying organisms crucial for carbon sequestration. Considering these documented changes in  
135 diverse oceanic regions and the critical nature of the SSTC around 40°S in the Atlantic Ocean, it  
136 is plausible that similar dynamics will impact the BCP in this region.

137  
138 In this study, we aim to quantify changes in the biological carbon pump at 40°S in the Atlantic  
139 Ocean. We leverage data from the GEOTRACES 40°S cruise, the first zonal expedition at this  
140 latitude in the South Atlantic to measure DIC. We join up all the other GLODAPv2.2022 cruises  
141 going perpendicularly and recent autonomous marine observations from the BGC-Argo array  
142 into a single analysis. This time series of marine carbonate chemistry measurements is used to  
143 calculate the rates of change in key variables and used to disentangle changes in the natural  
144 components of DIC (carbonate pump, C<sub>carb</sub> and soft tissue pump, C<sub>soft</sub>) from anthropogenic CO<sub>2</sub>  
145 (C<sub>anth</sub>). We examine the underlying reasons for the divergence in BCP estimations, probing into  
146 the shifts in water mass composition within formation areas and delving into the effects of  
147 diminished oxygenation and heightened remineralization in the Southern Ocean. BCP estimates  
148 are then aligned with global carbon budgets, highlighting potential gaps in our understanding of  
149 the biological carbon pump's inclusion in these estimates.

## 150 2 Materials and Methods



151  
152 **Figure 1.** Map of the study region in the South Atlantic Ocean. Red line with crosses show the  
153 trajectory of the longitudinal GEOTRACES 40°S cruise. Black triangles show the location of  
154 GLODAPv2.2022 cruises. Red dots show BGC-Argo float data. Color scale shows Chl-a  
155 concentration (log-scale; Chl-a data downloaded from CMEMS following Sauzède et al. (2016)).

### 156 2.1 Discrete measurements from GLODAPv2.2022

157 Data from 11 cruises along latitude 40°S in the Atlantic Ocean were extracted from the Global  
158 Ocean Data Analysis Project version 2 (GLODAPv2.2022; Lauvset et al. (2022), Fig. 1; see  
159 Table 1 in supplementary information) and analyzed. From these, only the GEOTRACES 40°S  
160 cruise occupied the entire latitudinal transect (Expocode #740H20111224, 2011, RRS James

161 Cook; cruise #4095 in GLODAPv2.2022) while the rest either covered it partially, or crossed it  
162 latitudinally. Only stations with a bottom depth beyond 1000 m were considered, as to remove  
163 data falling on the continental shelf and/or slope. Rather than using original cruise data, the  
164 analysis benefited from the GLODAPv2.2022 applied adjustment of properties, making the  
165 analysis internally consistent. Hydrographic parameters included temperature ( $T$ ), salinity ( $S_P$ ),  
166 dissolved oxygen ( $[O_2]$ ), dissolved inorganic carbon (DIC), total alkalinity ( $A_T$ ) and nitrate  
167 ( $NO_3^-$ ). Only data with a quality control deemed “Good” (Flag = 2) were used. This analysis  
168 considered the full depth of the water column, with an emphasis on the central and intermediate  
169 waters during the discussion as most change has been observed in these waters (Piñango et al.,  
170 2022).

## 171 **2.2 Autonomous data from BGC-Argo floats**

172 Float data were downloaded from the Argo Global Data Assembly Centre (AOML) for a 8-year  
173 period (2015 – 2023). Only months matching GLODAPv2.2022 were kept (i.e. October,  
174 November, December, January, February and March). Selected floats all fell within a defined  
175 geographical area matching GLODAPv2.2022 (38°S to 42°S, 15°W to 50°E, Fig. 1). All selected  
176 float profiles included temperature ( $T$ ), practical salinity ( $S_P$ ), dissolved oxygen ( $[O_2]$ ), pH on the  
177 total scale ( $pH_T$ ) and nitrate ( $NO_3^-$ ) (i.e. 9 floats, 73 profiles; see Table 2 in supplementary  
178 information). All BGC-Argo profiles used here were downloaded as Delayed Mode files which  
179 are designed for scientific exploitation and represent the highest quality of data to possibly  
180 extract climate-related trends (Bittig et al., 2019). Only adjusted data that were flagged as  
181 “Good” (QC=1) were used in this study, except for  $T$  and  $S_P$ , for which estimated values (QC=8)  
182 were used when adjusted data was missing. Each float profile was treated as the equivalent of a  
183 GLODAPv2.2022 cruise in the analysis.

## 184 **2.3 Derived variables**

185 For all BGC-Argo profiles,  $A_T$  was calculated using Python SciPy nonlinear least-square fitting  
186 (v.1.9.3; Virtanen et al., 2020), with  $T$ ,  $S_P$  and depth as input parameters. More information can  
187 be found in the supplementary information, along with a comparison to Lee et al. (2006)  $A_T$   
188 estimates (supp. info., Figs. B1, B2 and B3).

189  
190 Neutral density surfaces ( $\sigma^n$ ) were calculated from  $T$ ,  $S_P$ , pressure, latitude and longitude using  
191 the EOS-80 Legacy toolbox for MATLAB® (MathWorks®, USA). Absolute salinity ( $S_A$ ) and  
192 potential temperature ( $\theta$ ) were calculated from  $T$ ,  $S_P$ , and pressure using the Gibbs-SeaWater  
193 Oceanographic Toolbox for MATLAB® (MathWorks®, USA). Apparent oxygen utilization  
194 (AOU) was calculated from  $\theta$ ,  $S_A$  and  $[O_2]$  using the combined fit coefficients from Garcia and  
195 Gordon (1992). These calculations were carried out for all datasets without above variables  
196 either already measured or calculated.

197

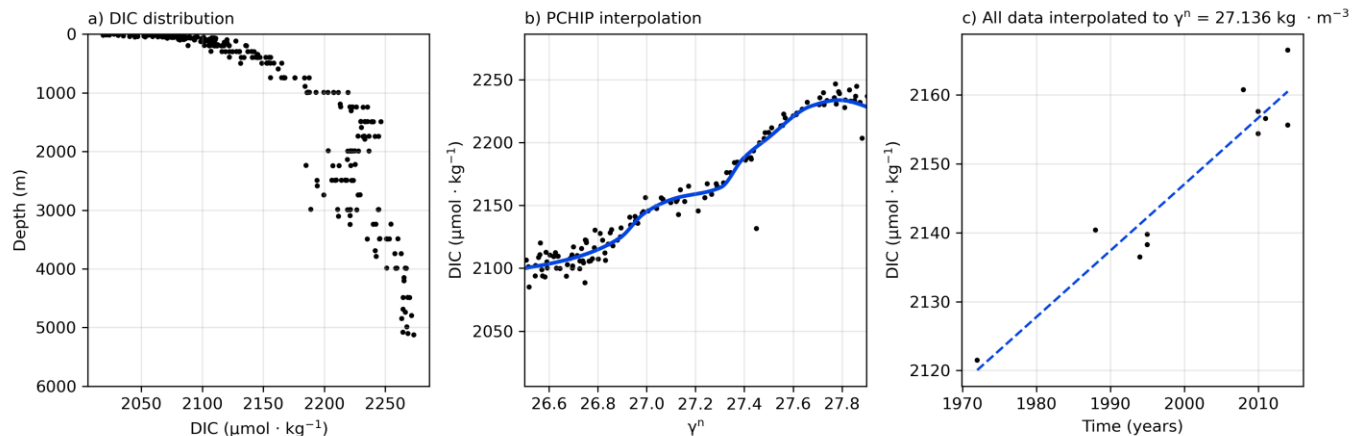
198 The Mixed Layer Depth (MLD) for each station during the GEOTRACES 40°S cruise  
199 was determined using a density criterion, with density calculated from  $T$ ,  $S_P$ , and pressure data  
200 according to the Python implementation of the Gibbs SeaWater (GSW) Oceanographic Toolbox  
201 of TEOS-10 (v. 3.6.16; McDougall and Barker (2011)). The MLD was defined as the depth at  
202 which the water's density increases by  $0.03 \text{ kg m}^{-3}$  compared to the surface. Then, the mean

203 MLD and mean neutral density across all stations for that cruise was calculated, resulting in a  
204 MLD of 54m ( $\gamma^n \approx 25.8$ ). 2.4 Marine carbonate system parameters

205 Depending on available variables, remaining marine carbonate parameters were calculated from  
206 any pair of DIC,  $A_T$ ,  $pH_T$  using PyCO2SYS v1.8.1 (Humphreys et al., 2022), and with the  
207 carbonic acid dissociation constants from Sulpis et al. (2020), bisulfate dissociation constant  
208 from Dickson (1990), the total boron:chlorinity from Uppström (1974) and the hydrogen fluoride  
209 dissociation constant from Dickson and Riley (1979). When available, phosphate and silicate  
210 were included in the carbonate system calculations but their inclusion did not affect the results  
211 significantly as their concentrations are relatively low in the open ocean. Calculated parameters  
212 include pH on the total scale ( $pH_T$ ) and the seawater partial pressure of  $CO_2$  ( $pCO_2$ ) for  
213 GLODAPv2.2022 data, and DIC and  $pCO_2$  for BGC-Argo data.

## 214 2.5 Interpolations

215 For each year, all variable data were clustered and interpolated vertically to  $\gamma^n$  levels using  
216 Piecewise Cubic Hermite Interpolating Polynomial (PCHIP) fits to observations (Fritsch &  
217 Carlson, 1980; Humphreys et al., 2016). Briefly, the PCHIP method uses monotonic cubic  
218 splines to find the value of new points. This allows for comparability between all cruises across  
219 the transect as averaging on isopycnals mimics real oceanic mixing processes occurring  
220 primarily along isopycnals, or, more precisely, along neutral density surfaces. Data were not  
221 extrapolated beyond the measured observational  $\gamma^n$  levels.



222  
223 **Figure 2.** Analysis routine for each cruise and float profile, here showing for GEOTRACES  
224 40°S longitudinal cruise: a) the vertical distribution of DIC; b) the PCHIP interpolation for DIC  
225 along neutral density levels; and c) the linear regression at a given neutral density level.

## 226 2.6 Rates of change

227 For each variable, ordinary least square regressions were used to determine their rate of change  
228 at each  $\gamma^n$  level. All rates of change are reported as  $\frac{dX}{dt} \pm U$ , where  $X$  is the variable and  $U$  is the  
229 associated uncertainty. Regressions were achieved using Python library SciPy v.1.9.3 (Virtanen  
230 et al., 2020). All rates of change were calculated with the same time range for all variables, that  
231 is from 1972 to 2023, except for silicate for which only GLODAPv2.2022 data is available up to  
232 2014.

233 **2.7 CO<sub>2</sub> components**

234 Three pumps contribute to the distribution of DIC: photosynthesis, respiration and  
 235 remineralization(  $C_{soft}$ ), the formation and dissolution of calcium carbonate (  $C_{carb}$ ) and the  
 236 uptake of natural and anthropogenic CO<sub>2</sub> (  $C_{anth}$ ; Gruber et al., 1996; Volk & Hoffert, 1985.  
 237 Thus, DIC changes can be described as:  
 238

$$\Delta T_C = \Delta C_{soft} + \Delta C_{carb} + \Delta C_{sol} \quad (1).$$

239 Biological activity is responsible for converting dissolved inorganic nutrients to particulate  
 240 organic matter. These particles are transported down the water column through gravitational  
 241 settling and active transport by marine organisms. During their settling to deeper waters, carbon  
 242 and nutrients are returned to their dissolved, inorganic forms through remineralization while  
 243 taking up O<sub>2</sub> and thus increasing AOU (Redfield, 1963). This process drives the soft tissue  
 244 pump, which is defined as:  
 245

$$\Delta C_{soft(AOU)} = -R_{C/O_2} \cdot \Delta AOU \quad (2a),$$

$$\Delta C_{soft(NO_3)} = R_{C/NO_3^-} \cdot \Delta NO_3^- \quad (2b),$$

246 where  $R_{C/X}$  is the increase in  $C$  as a fraction of X variable consumption during remineralization.  
 247 In this study, we used the ratio from Anderson and Sarmiento (1994) as follows:  
 248

$$\begin{array}{l} \text{P: N: C: } -O_2 \\ 1: 16: 117: 170 \end{array} \quad (3),$$

249 Thus,  $R_{C/O_2}$  and  $R_{C/NO_3^-}$  can be assumed to be a constant value of  $-0.688 \pm 0.092$  and  $7.31 \pm 0.092$   
 250 respectively (Anderson & Sarmiento, 1994).  
 251

252 The formation and dissolution of CaCO<sub>3</sub> makes up the carbonate pump, where an increase in  $C$  is  
 253 coupled with an increase in A<sub>T</sub> of double the magnitude (Wolf-Gladrow et al., 2007):  
 254

$$\Delta C_{carb} = 0.5 \cdot (\Delta A_T - R_{N/O_2} \cdot \Delta NO_3^-) \quad (4),$$

255 where  $R_{N/O_2}$  is a ratio of  $-0.0941 \pm 0.0081$  (Anderson & Sarmiento, 1994).  
 256

257 The remaining term, namely the solubility pump, relies on the uptake of anthropogenic CO<sub>2</sub>  
 258 ( $\Delta C_{anth}$ ) and the CO<sub>2</sub> air-sea disequilibrium ( $\Delta C_{diseq}$ ) at the time the water lost contact with the  
 259 atmosphere (Gruber et al., 1996). Assuming  $\Delta C_{diseq} = 0$ , i.e. no significant long-term trend in  
 260 air-sea CO<sub>2</sub> disequilibrium, the accumulated anthropogenic  $\Delta C_{anth}$  is defined as:  
 261

$$\Delta C_{anth} = \Delta C_{sol} - \Delta C_{diseq} \approx \Delta C_{sol} \quad (5).$$

262

## 2.8 Natural CO<sub>2</sub> inventory change

263 Changes in  $C_{\text{soft(AOU)}}$  and  $C_{\text{soft(NO}_3\text{)}}$  were multiplied by a density factor of 1028 to convert units  
264 from  $\mu\text{mol kg}^{-1} \text{ yr}^{-1}$  to  $\mu\text{mol m}^3 \text{ yr}^{-1}$ . Resulting values were integrated along the water column by  
265 sum ( $C_{\text{soft(AOU)-int}}$  and  $C_{\text{soft(NO}_3\text{)-int}}$ ). Assuming lateral homogeneity,  $C_{\text{soft(AOU)-int}}$  and  $C_{\text{soft(NO}_3\text{)-int}}$   
266 were further converted to  $\text{GtC m}^2 \text{ yr}^{-1}$  and integrated over the surface of the study area.

267

## 2.9 Uncertainty propagation

268 For GLODAPv2.2022, uncertainties were assigned based on Table 3 of Lauvset et al. (2022) for  
269 all data dated from after 1994 (i.e. first use of CRMs). For data prior to 1994, an uncertainty of  
270  $\pm 17.2 \mu\text{mol kg}^{-1}$  was assigned (Dickson, 1992). Most BGC-Argo floats included the error for  
271 each adjusted variable. Some uncertainties were missing for T and S<sub>p</sub>, for which values were  
272 assigned based on Williams et al. (2017) and Mignot et al. (2019), except for the calculated A<sub>T</sub>  
273 for which the fit RMSE was used ( $5.5 \mu\text{mol kg}^{-1}$ , see Section B in supplementary information).  
274 Uncertainties for variables calculated with PyCO2SYS v1.8.1 were propagated using the  
275 independent uncertainty argument (Humphreys et al., 2022).

276

277 In the process of quantifying analysis uncertainty, a multifaceted approach was employed to  
278 ensure comprehensive error propagation. To assess the uncertainty in the rates of change, a  
279 differential analysis was undertaken, calculating the derivatives for all variables under  
280 consideration (i.e. forward-finite differences). Each variable was incrementally altered, specific  
281 to the variable's nature, and the impact of these perturbations on the overall outcome was studied  
282 through another linear regression on the modified dataset. The differences between the  
283 coefficients of the original and modified datasets provided insights into the sensitivity of each  
284 variable. After normalization, these differences gave the true derivatives. By juxtaposing these  
285 derivatives with known measurement uncertainties, a comprehensive error term for each  
286 variable's rate of change was determined, offering a robust assessment of propagated  
287 uncertainties. This step provided a foundational understanding of how minor perturbations in  
288 each variable could influence the outcome.

289

290 Subsequently, to further refine the understanding of the variability and potential uncertainties  
291 inherent in the dataset, a bootstrapping technique was applied. Essentially, the data for specific  
292 cruises was selectively omitted in a series of simulations, creating a variety of modified datasets.  
293 This non-parametric statistical method facilitated the estimation of the distribution of sample  
294 statistics by resampling with replacement, thereby offering insights into the potential variability  
295 of the results.

296

297 Finally, for each measured variable, an internal bias was determined for each cruise or float  
298 profile using the standard deviation of each linear regression from the rates of change estimation.  
299 All uncertainties were then synthesized to produce a combined error estimate. This layered  
300 approach ensured a robust assessment of analysis uncertainty, capturing both the immediate  
301 sensitivities of the variables and the broader variability in the dataset.

302

## 3 Results

303 Multi-decadal rates of change for all available and derived carbonate parameters were calculated  
304 using GLODAPv2.2022 and BGC-Argo data along latitude 40°S for the period 1972-2023.

305 Changes in individual variables are reported in Fig. 3, while the calculated change in each  
306 component of DIC is shown in Fig. 4. For all variables, little to no change was observed deeper  
307 than ~2000 m in the water column thus only data down to this depth are presented here.

308

309 On average, surface waters became warmer and fresher, which was reflected in  $A_T$  with a slight  
310 negative change. Slight decreases of  $-0.04 \pm 0.0006 \text{ }^\circ\text{C yr}^{-1}$  in  $\theta$  and  $-0.01 \pm 0.0002 \text{ yr}^{-1}$  in  $S_p$   
311 were observed in the top ~300 m ( $\gamma^n < 27.0 \text{ kg m}^{-3}$ ), with virtually no change deeper in the water  
312 column (Fig. 3a-b). This was closely mirrored by  $A_T$ , which showed a maximum decrease of -  
313  $0.49 \pm 0.11 \text{ } \mu\text{mol kg}^{-1} \text{ yr}^{-1}$  within the top ~200 m ( $\gamma^n < 26.8 \text{ kg m}^{-3}$ ), while showing no change  
314 deeper in the water column (Fig. 3c).

315

316 Surface waters also showed signs of deoxygenation and increased AOU (Fig. 3h), while the  
317 nitrate pool increased (Fig. 3i).  $[\text{O}_2]$  decreased down to ~900m ( $\gamma^n \approx 27.4 \text{ kg m}^{-3}$ ), with a  
318 minimum  $\Delta[\text{O}_2]$  of  $-0.56 \pm 0.05 \text{ } \mu\text{mol kg}^{-1} \text{ yr}^{-1}$  (Fig. 3g). Deeper than 150 m, AOU increased by a  
319 maximum of  $+0.54 \pm 0.02 \text{ } \mu\text{mol} \cdot \text{kg}^{-1} \cdot \text{yr}^{-1}$ , from the surface down to ~2000 m ( $\gamma^n \approx 27.9 \text{ kg m}^{-3}$ ;  
320 Fig. 3h-i). Both AOU and  $[\text{O}_2]$  converged towards no change at around ~300 m ( $\gamma^n \approx 27.0 \text{ kg m}^{-3}$ ),  
321 before continuing their respective decrease/increase. An important increase in  $\text{NO}_3^-$  was  
322 observed with a peak of  $+0.14 \pm 0.01 \text{ } \mu\text{mol} \cdot \text{kg}^{-1} \cdot \text{yr}^{-1}$  for the first ~150m ( $\gamma^n < 26.7 \text{ kg m}^{-3}$ ),  
323 while slowly converging towards no change by ~1000m ( $\gamma^n \approx 27.5 \text{ kg m}^{-3}$ ; Fig. 3i).

324

325 It's important to note that for the analysis of the N/P ratio and  $[\text{Si}]$ , the data is limited to  
326 measurements up to 2014. This limitation arises because the BGC-Argo floats are not equipped  
327 to measure phosphate and silicate, thus only GLODAPv2.2022 data was used. Nonetheless,  
328 within this dataset, there was no significant change observed in the N/P ratio (Fig. 3l).  
329 Additionally,  $[\text{Si}]$  displayed an increase of  $+0.15 \pm 0.08 \text{ } \mu\text{mol} \cdot \text{kg}^{-1} \cdot \text{yr}^{-1}$  near  $\gamma^n = 27.4$ , with no  
330 substantial alterations observed in the remaining portions of the water column (Fig. 3k).

331

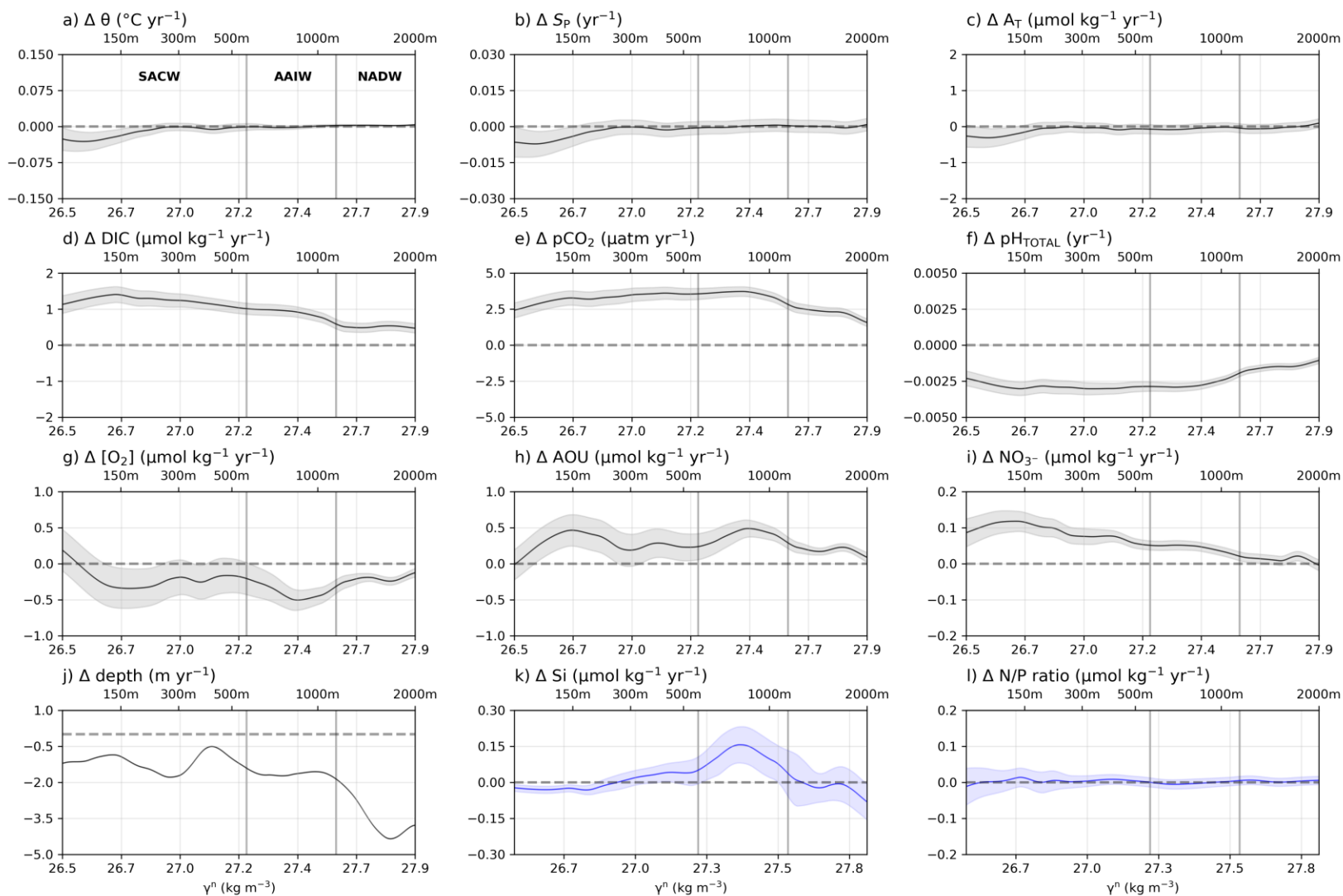
332 Seawater at 40°S became more acidic due to a change in DIC partially caused by biological  
333 processes, calcium carbonate formation and  $\text{CO}_2$  uptake. A small decrease of  $-0.24 \pm 0.06$   
334  $\mu\text{mol kg}^{-1} \text{ yr}^{-1}$  in the carbonate pump,  $C_{\text{carb}}$ , was observed within the first ~200m ( $\gamma^n < 26.8 \text{ kg m}^{-3}$ )  
335 of the water column (Fig. 4), correlating closely with the change in  $A_T$  (Fig. 3c). DIC showed  
336 an increase above ~2000 m ( $\gamma^n \approx 27.9 \text{ kg m}^{-3}$ ; Fig. 3d and Fig. 4) with a maximum  $+1.44 \pm 0.11$   
337  $\mu\text{mol kg}^{-1} \text{ yr}^{-1}$  in the surface waters ( $\gamma^n \approx 26.7 \text{ kg m}^{-3}$ ; Fig. 3d and Fig. 4). It is interesting to note  
338 that the change in DIC was higher down to 2000m when using all available data, most likely  
339 indicative of a deeper penetration depth within the last decade, and noticeable thanks to the high-  
340 resolution of BGC-Argo data. Seawater  $p\text{CO}_2$  showed a corresponding average increase of  $+3.83$   
341  $\pm 0.15 \text{ } \mu\text{atm yr}^{-1}$ , before slowly converging back to no change deeper than 2000 m ( $\gamma^n \approx 27.9 \text{ kg m}^{-3}$ ;  
342 Fig. 3e). These changes were closely followed by an average decrease of  $-0.002 \pm 0.0001 \text{ yr}^{-1}$   
343 in  $\text{pH}_T$  and a maximum decrease of  $-0.003 \pm 0.0001 \text{ yr}^{-1}$  in the shallow subsurface (~150 m,  $\gamma^n$   
344  $< 26.7 \text{ kg m}^{-3}$ ; Fig. 3f), where the pH maximum is often located (Arroyo et al., 2022). This  
345 change in  $\text{pH}_T$  is consistent with most recent globally averaged rate of surface ocean pH change,  
346  $-0.0016 \pm 0.0006 \text{ yr}^{-1}$  (Garcia-Soto et al., 2021).

347

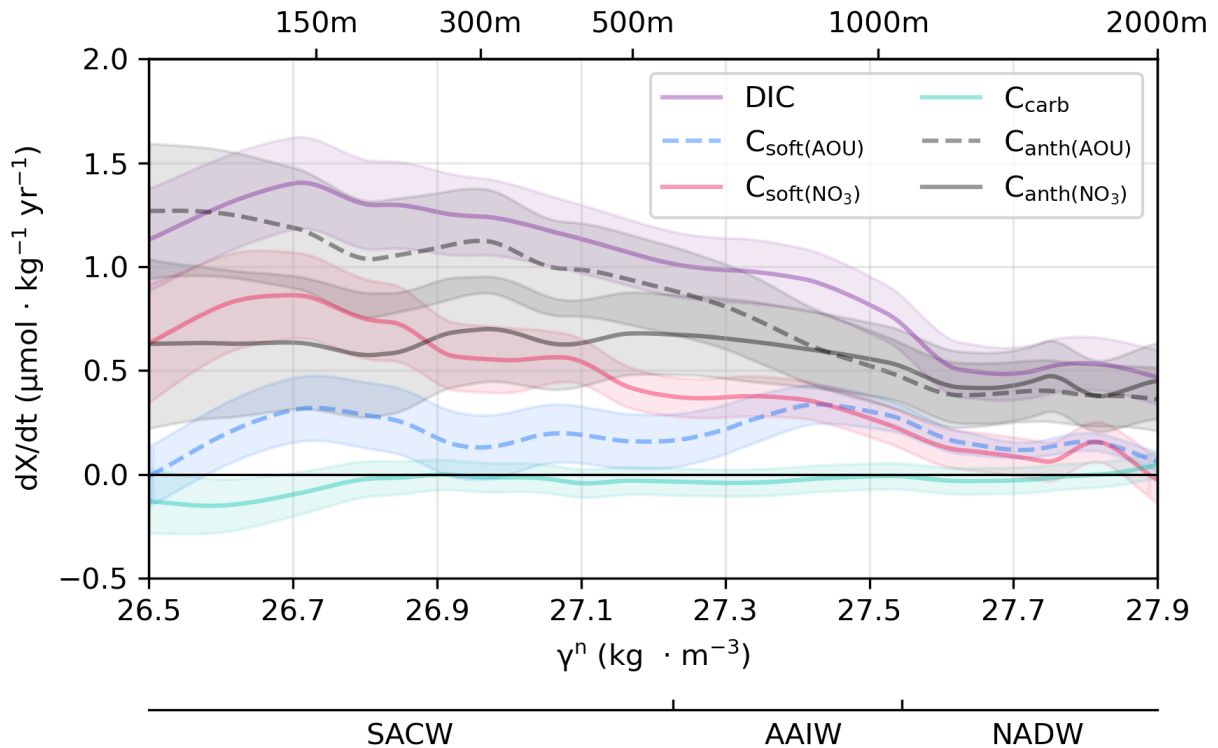
348 Change in DIC appears to be mostly caused by an accumulation of  $C_{\text{anth}}$ , in the surface waters,  
349 which was further supported by a parallel increase in seawater  $p\text{CO}_2$  (Figs. 3e and Fig. ). Not all  
350 DIC change was attributed to  $C_{\text{anth}}$ , as there also appeared to be a significant increase in the soft

351 tissue pump (Fig. 4). If calculated using AOU,  $C_{\text{soft(AOU)}}$  increased by  $+0.20 \pm 0.03 \mu\text{mol} \cdot \text{kg}^{-1} \cdot$   
352  $\text{yr}^{-1}$  down to  $\sim 2000\text{m}$  ( $\gamma^n \approx 27.9 \text{ kg m}^{-3}$ ; Fig. 4), while being close to no change near  $\sim 300 \text{ m}$  ( $\gamma^n \approx$   
353  $27.0 \text{ kg m}^{-3}$ ; Fig. 4). The corresponding  $C_{\text{anth(AOU)}}$  thus represented most of the DIC change, with  
354 an increase of  $+1.48 \pm 0.13 \mu\text{mol} \cdot \text{kg}^{-1} \cdot \text{yr}^{-1}$  close to the surface ( $\gamma^n < 26.7 \text{ kg m}^{-3}$ ; Fig. 4).  
355 However, if calculated using  $\text{NO}_3^-$ ,  $C_{\text{soft(NO}_3\text{)}}$  showed an increase  $\sim 4$  times greater than  $C_{\text{soft(AOU)}}$ ,  
356 with  $+0.85 \pm 0.07 \mu\text{mol kg}^{-1} \text{ yr}^{-1}$  in the surface waters ( $\gamma^n < 26.8 \text{ kg m}^{-3}$ ; Fig. 4), and  $C_{\text{anth(NO}_3\text{)}}$   
357 then contributing half of  $C_{\text{anth(AOU)}}$ , with an average increase of  $+0.67 \pm 0.14 \mu\text{mol kg}^{-1} \text{ yr}^{-1}$  down  
358 to  $1000 \text{ m}$  ( $\gamma^n \approx 27.5 \text{ kg m}^{-3}$ ; Fig. 4).

359  
360 The depth-integrated increase in the soft tissue pump was approximately  $+0.004 \pm 0.002 \text{ GtC yr}^{-1}$   
361 for  $C_{\text{soft(AOU)}}$  and  $+0.006 \pm 0.002 \text{ GtC yr}^{-1}$  for  $C_{\text{soft(NO}_3\text{)}}$  within the study area.  
362



363  
 364 **Figure 3.** Change in biogeochemical parameters across 40°S in the Atlantic Ocean for all available data. Approximate depths are  
 365 shown at the top of each plot, along water masses as part of subplot a. Note that blue panels k and l only include data up to 2014 as  
 366 BGC-Argo floats are not equipped for phosphate and silicate measurements. MLD is off the x-axis (54m,  $\gamma^n \approx 25.8$ ).



367 **Figure 4.** Rates of change in DIC (purple) and its components,  $C_{\text{carb}}$  (turquoise),  $C_{\text{soft}(\text{NO}_3)}$   
 368 estimated from  $\text{NO}_3^-$  (red),  $C_{\text{soft}(\text{AOU})}$  estimated from AOU (dashed blue), with corresponding  
 370  $C_{\text{anth}(\text{NO}_3)}$  in solid black and  $C_{\text{anth}(\text{AOU})}$  in dashed black. Results are for the compilation of all  
 371 available data. Approximate depths are showed at the top and water masses at the bottom of the  
 372 axes. MLD is off the x-axis (54m,  $\gamma^n \approx 25.8$ ).

## 373 4 Discussion

374 Although the biological pump at  $40^\circ\text{S}$  has clearly increased, the magnitude remains uncertain,  
 375 depending on whether  $\text{NO}_3^-$  or AOU is used to estimate the soft tissue pump component. Below,  
 376 we discuss this uncertainty and the implications of our findings, first looking at the physical  
 377 factors and subsequently the influence of biology.

### 378 4.1 Influence of Physical Factors on BCP Dynamics

#### 379 4.1.1 Melting Ice

380 Variability in oxygen content at  $40^\circ\text{S}$  is largely influenced by sea ice dynamics affecting gas  
 381 exchange, temperature and salinity (Hofmann et al., 2011). The stratification induced by  
 382 meltwater creates a barrier that inhibits deep water mixing. As a result, vertical water exchange  
 383 between the surface and deeper ocean layers is slowed, retaining carbon and nutrients in the  
 384 upper water column for longer, marking a transition from a system that exports carbon and  
 385 nutrients to one that retains them (Gjelstrup et al., 2022; Priest et al., 2023; von Appen et al.,  
 386 2021). However, the melting of sea ice cools seawater, enhancing the solubility of  $\text{CO}_2$  and  $\text{O}_2$   
 387 without affecting  $\text{NO}_3^-$ . Subsequent air-sea gas exchange will thereby increase DIC and  $[\text{O}_2]$ , but

388 it will not alter AOU, because  $[O_2]$  changes to match its new saturation level ( $[O_2]_{\text{sat}}$ ). The  
389 impact varies with the supersaturation or undersaturation of surface waters with respect to  
390 atmospheric  $CO_2$  and  $O_2$  (Council, 2010; Figuerola et al., 2021). In scenarios of reduced gas  
391 exchange due to diminished sea ice in the Southern Ocean, there should be a decrease in DIC and  
392 AOU, as the melting sea ice enhances the ocean's capacity to absorb atmospheric  $CO_2$  and  $O_2$ ,  
393 which would lead the concentrations of these dissolved gases to increase thus changing  $C_{\text{softAOU}}$   
394 but not  $NO_3^-$  and  $C_{\text{soft}(NO_3)}$ .

395  
396 Melting land ice also enhances ocean stratification and introduces micronutrients like iron,  
397 fueling biological productivity in near-surface waters (Lannuzel et al., 2010; Lannuzel et al.,  
398 2016; Morley et al., 2020). Sediment-derived iron, accounting for  $54 \pm 15\%$  of total iron flux, is  
399 carried from continental shelves via benthic diffusion and sediment resuspension (De Jong et al.,  
400 2012; Tian et al., 2023). This transport may influence nutrient dynamics and productivity as far  
401 as 3500 km from the Antarctic Peninsula (De Jong et al., 2012). An influx of micronutrients  
402 leads to a higher uptake of DIC and also nitrate  $NO_3^-$ , resulting in an decrease in  $C_{\text{soft}(NO_3)}$ . These  
403 changes, predominantly affecting near-surface photosynthesis, align with the Redfield Ratio,  
404 which predicts a decrease in  $NO_3^-$  proportional to the decrease in DIC. However, this would  
405 impact AOU and hence also  $C_{\text{soft}(AOU)}$  less because  $O_2$  more quickly re-equilibrates with the  
406 atmosphere than DIC. Enhanced remineralization at greater depths due to the increased  
407 productivity would change DIC, AOU and  $NO_3^-$  in line with the Redfield ratio (Henley et al.,  
408 2020). As the composition of the water we observe at  $40^\circ S$  is the result of transport of this water  
409 from south to north it also reflects the initial preformed value from the enhanced productivity  
410 near the Antarctic as well as processes happening at  $40^\circ S$  and during transport (Morley et al.,  
411 2020).

412  
413 A component of the observed increase in DIC at  $40^\circ S$  could hence reflect both melting of sea  
414 and land ice, which in turn impact the BCP. But unlike for  $NO_3^-$ , the AOU change from  
415 increased productivity is quickly erased by air-sea gas exchange. Changes in AOU observed at  
416  $40^\circ S$  therefore cannot result from these melting processes, while the changes in  $NO_3^-$  could stem  
417 from these changing endmember conditions.

#### 418 **4.1.2 Interior ocean mixing**

419 Recent studies have highlighted changes in ocean circulation patterns, which most likely are also  
420 reflected at  $40^\circ S$ . Decrease in the ages of Subantarctic Mode Water (SAMW) and Circumpolar  
421 Deep Water (CDW) were observed across the South Atlantic Ocean since the 1990s, suggesting  
422 enhanced ventilation, a phenomenon partly attributed to shifts in westerly winds (Fine et al.,  
423 2017; Tanhua et al., 2017; Waugh et al., 2013). This trend in SAMW indicates potentially  
424 increased isopycnal mixing, which elevates surface DIC due to the upward transport of DIC-rich  
425 deep waters which may drive part of the observed increase in DIC at  $40^\circ S$  (Fig. 3d).

426 Additionally, Wei et al. (2022), focusing on a transect from the Rio Grande Rise to the Mid-  
427 Atlantic Ridge, demonstrated increases in diapycnal diffusivities, again indicating intensified  
428 mixing, thus implying enhanced vertical circulation of nutrient-rich deep waters. This  
429 observation is consistent with the observed rise in  $NO_3^-$  and  $C_{\text{soft}(NO_3)}$  at  $40^\circ S$  (Fig. 3i and 4).  
430 Both the isopycnal and diapycnal mixing introduce oxygen-poor deep water to the surface,  
431 increasing SACW AOU, especially in regions with high remineralization (Fig.3h; Fine et al.,  
432 2017; Tanhua et al., 2017; Waugh et al., 2013. This suggests that the apparent increase in

433 remineralization within the BCP as inferred from DIC, AOU, and  $\text{NO}_3^-$  measurements, is  
434 primarily due to the enhanced advection of older deep waters to the surface.

435  
436 Piñango et al. (2022) also reported increased organic matter remineralization in the AAIW likely  
437 indicating deoxygenation. This is due to an enhanced flux of organic matter, which increases  
438 microbial oxygen consumption, and enhanced ventilation. While the latter introduces oxygen, it  
439 also brings in more anthropogenic carbon, exacerbating the oxygen demand for remineralization.  
440 This is especially true along the AAIW from  $50^\circ\text{S}$  to  $30^\circ\text{S}$  where increased AOU was observed  
441 at a mean rate of AOU change of  $0.23 \pm 0.68 \mu\text{mol kg}^{-1} \text{ yr}^{-1}$  south of  $30^\circ\text{S}$  which concurs with  
442 our results (Fig. 3; Piñango et al., 2022). This is consistent with the deoxygenation trend reported  
443 by Santos et al. (2016) for the AAIW in the South Atlantic subtropical gyre from 1960 to 2015,  
444 which was  $-0.18 \pm 0.04 \mu\text{mol kg}^{-1} \text{ yr}^{-1}$ . It also aligns with the AOU rate observed by Fontela  
445 et al. (2021) in the Argentine Basin, which was  $0.38 \pm 0.13 \mu\text{mol kg}^{-1} \text{ yr}^{-1}$ . Additionally, these  
446 results agree with the AAIW deoxygenation documented by Schmidtke et al. (2017) over the last  
447 two decades.

448  
449 A component of the observed changes in DIC, AOU,  $\text{NO}_3^-$  and therefore the BCP at  $40^\circ\text{S}$  is thus  
450 mechanistically linked to enhanced mixing through an increased influence of deeper waters on  
451 overlying water masses.

#### 452 **4.1.3 Wind-driven circulation**

453 Increased wind-driven circulation has been invoked to explain changes in marine  
454 biogeochemical cycles, including effects on DIC and nutrients (England et al., 2014; Keppler &  
455 Landschützer, 2019; Liu et al., 2023).

456  
457 The rate of gas exchange between the ocean and atmosphere is controlled by a set of physical  
458 processes that scale with wind speed (Wanninkhof, 2014). Because the South Atlantic Ocean is a  
459 net sink for  $\text{CO}_2$  (i.e., seawater  $p\text{CO}_2$  is lower than atmospheric  $p\text{CO}_2$ ), enhanced gas exchange  
460 due to stronger surface winds would increase surface ocean  $p\text{CO}_2$  and DIC. The same process  
461 decreases AOU, which is positive in surface waters here (Fig. 3h), due to the absorption of  
462 atmospheric oxygen. In contrast, dissolved nutrients such as  $\text{NO}_3^-$  (and therefore  $C_{\text{soft}(\text{NO}_3)}$ ),  
463 which are primarily controlled by biological uptake and nutrient cycling, are not directly affected  
464 by intensified gas exchange.

465  
466 However, increased winds also drive enhanced upwelling. Deep waters are high in DIC, AOU  
467 and  $\text{NO}_3^-$  due in a large part to remineralization of organic matter, so enhanced upwelling  
468 elevates all these properties in the SACW roughly in line with the Redfield ratio (Fig. 3d,h,i;  
469 England et al., 2014; Liu et al., 2023). Accordingly, changes in wind-driven circulation would  
470 increase both  $C_{\text{soft}(\text{NO}_3)}$  and  $C_{\text{soft}(\text{AOU})}$  in SACW, but likely in agreement with the Redfield ratio  
471 and true change in  $C_{\text{soft}}$ . This aspect therefore cannot cause the observed discrepancy between  
472  $C_{\text{soft}(\text{NO}_3)}$  and  $C_{\text{soft}(\text{AOU})}$  observed at  $40^\circ\text{S}$ .

473  
474 Additionally, increased mixing due to stronger winds leads to a more uniform distribution of  
475 DIC in the upper part of the water column as the surface mixed layer thickens (England et al.,  
476 2014), as seen at  $40^\circ\text{S}$  (Fig. 3j). This mixing increases AOU near the surface and lowers it at  
477 depth. Mixing also results in a more even distribution of nutrients like  $\text{NO}_3^-$  throughout the water

478 column, redistributing these vertically rather than straightforwardly increasing or decreasing the  
479 soft tissue pump.

#### 480 **4.2 Biological effects on quantifying the BCP**

481 The increase in  $\text{NO}_3^-$  at  $40^\circ\text{S}$ , especially in the first 500m (Fig. 3i), could reflect increased  
482 remineralization, possibly caused by enhanced organic matter export at  $40^\circ\text{S}$  (Boyd & Trull,  
483 2007; Sarmiento, 2006). This should be accompanied by an  $[\text{O}_2]$  decline in the same waters,  
484 increasing AOU, which in the surface mixed layer could then be attenuated by oxygen exchange  
485 with the atmosphere. Consequently,  $C_{\text{soft(AOU)}}$  in the near surface would underestimate the actual  
486 change in  $C_{\text{soft}}$ , while in deeper waters beneath the mixed layer (without the associated air-sea  
487 gas exchange causing a bias in  $C_{\text{soft(AOU)}}$ ),  $C_{\text{soft(AOU)}}$  would be consistent with  $C_{\text{soft(NO}_3)}$  (Fig. 4).  
488 However,  $C_{\text{soft(AOU)}}$  and  $C_{\text{soft(NO}_3)}$  differ significantly from each other down to around 800 m (or  
489  $27.4 \text{ kg m}^{-3}$ ), which is deeper than the mixed layer here (54m,  $\gamma^n \approx 25.8$ ), so this is not a complete  
490 explanation for the discrepancy.

491  
492 In shallower waters, other factors might explain the observed discrepancy between  $\Delta C_{\text{soft(AOU)}}$   
493 and  $\Delta C_{\text{soft(NO}_3)}$ , such as changes in the stoichiometry of organic matter. Variations from standard  
494 plankton biomass elemental ratios (i.e., the Redfield ratio; Redfield, 1958) have been observed  
495 spatially and temporally (Inomura et al., 2022; Martiny et al., 2013; Tanioka & Matsumoto,  
496 2020), which may contribute to the difference between  $C_{\text{soft(AOU)}}$  and  $C_{\text{soft(NO}_3)}$  observed here  
497 (Fig. 4; Anderson and Sarmiento, 1994). South of  $40^\circ\text{S}$ , the carbon to nitrogen (C:N) ratio is  
498 closely aligned with the Redfield ratio (Johnson et al., 2022). Conversely, north of  $40^\circ\text{S}$ ,  
499 dissolved organic matter (DOM) has higher C:N ratios, with  $10.4 \pm 4.1$  at  $30^\circ\text{S}$ ,  $14.0 \pm 4.8$  at  
500  $35^\circ\text{S}$ , and  $9.7 \pm 1.7$  at  $40^\circ\text{S}$ , all surpassing the Redfield ratio of 6.6 (Johnson et al., 2022). The  
501 elevated C:N observed at  $40^\circ\text{S}$  could then also result from a changing balance between water  
502 masses from the north and the south. Organic matter (OM) with higher C:N requires more oxygen  
503 for its remineralization, thereby accelerating the consumption of dissolved oxygen (Matsumoto  
504 et al., 2020; Szewczyk et al., 2023). Climate change is expected to cause significant  
505 stoichiometric shifts in plankton biomass, with warmer temperatures and rising  $\text{CO}_2$  levels  
506 promoting higher C:P and N:P ratios (Ayo et al., 2017; DeVries, 2018; DeVries et al., 2017;  
507 Toseland et al., 2013; van de Waal et al., 2010; Yvon-Durocher et al., 2017) which may result in  
508 increased oxygen consumption during remineralization and thus higher AOU (DeVries, 2018).  
509

510 The enhanced remineralization and possible changes in C:N observed at  $40^\circ\text{S}$  may be due to  
511 increased diatom populations further south (Arrigo et al., 1999; Arrigo et al., 2015; Soppa et al.,  
512 2016). Diatoms are reliant on silicate and significant nitrate consumers. Also enhanced inputs of  
513 iron are known to stimulate diatom productivity (Sect. 4.1.1). Diatoms secrete transparent  
514 exopolymeric particles (TEP), which act like glue to hold aggregates together, leading to faster  
515 sinking of marine particles and a more efficient biological pump (Chen & Thornton, 2015;  
516 Toullec & Moriceau, 2018). TEP production also increases the C:N ratio (Kim et al., 2021;  
517 Passow, 2002). Boosted silicate availability, most likely due to enhanced upwelling and glacial  
518 runoff (Henley et al., 2020), may accordingly reduce  $\text{NO}_3^-$  levels at the sea surface and increase  
519  $\text{NO}_3^-$  and AOU in the AAIW, due to enhanced sinking and remineralization of algal diatom  
520 biomass. If driven by diatoms, we would expect the increased  $\text{NO}_3^-$  and AOU in deeper waters to  
521 be accompanied by an increase in  $[\text{Si}]$  in AAIW (Cael et al., 2021), which is what we observe at  
522  $40^\circ\text{S}$  (Fig. 3k). Either through remote or via locally enhanced productivity an increased

523 abundance of diatoms, caused by higher iron and [Si], could be responsible for the changes in the  
524 BCP that we observe.

### 525 **4.3 Consequences of Changes in the Biological Carbon Pump**

#### 526 **4.3.1 Implications for Marine CO<sub>2</sub> Sink**

527 Previous studies have shown that the South Atlantic Ocean is a sink of atmospheric CO<sub>2</sub>, with an  
528 average net air-to-sea CO<sub>2</sub> flux of 0.3 Pg C yr<sup>-1</sup> (Takahashi et al., 1997; Takahashi et al., 2002).  
529 Recent work has highlighted strong seasonality in the South Atlantic CO<sub>2</sub> flux, acting as a strong  
530 sink during the spring when most primary production takes place, and shifting towards a source  
531 during autumn (Lencina-Avila et al., 2016; Padin et al., 2010). Monitoring whether the South  
532 Atlantic acts as a source or sink of CO<sub>2</sub> is vital for understanding its role in the global carbon  
533 cycle, as it directly influences the atmospheric CO<sub>2</sub> concentration and therefore Earth's climate  
534 (Lencina-Avila et al., 2016; Padin et al., 2010). As these variations are connected to the  
535 biological productivity of the South Atlantic Ocean, it is especially important to understand the  
536 biological pump's contribution to changes in DIC, which has a direct impact on whether the  
537 ocean basin acts as a source or sink of CO<sub>2</sub>.

538  
539 The observed increase in surface ocean pCO<sub>2</sub> at 40°S is consistent with the growth in  
540 atmospheric pCO<sub>2</sub> (Fig. 3e). If the changes in the BCP were to lead seawater pCO<sub>2</sub> to rise faster  
541 or slower than atmospheric pCO<sub>2</sub>, this would cause an decrease or increase respectively of the  
542 ocean CO<sub>2</sub> sink (DeVries et al., 2017).  
543

#### 544 **4.3.2 Carbon Export & BCP Role in Climate Responses**

545 Our findings at 40°S indicate that the biological pump is experiencing shifts due to a mix of  
546 chemical changes in water mass formation regions and biological factors across the Atlantic  
547 Ocean. Model results suggest that the anticipated increase in iron supply and improved light  
548 availability for phytoplankton—owing to enhanced near-surface stratification and prolonged ice-  
549 free periods—will likely amplify primary production. This could, in turn, boost carbon export  
550 around the Antarctic region (Henley et al., 2020). These observations at 40°S may be the early  
551 signs of the impacts of global change in the Southern Ocean.

552  
553 Building on these observations, the depth-integrated increase in organic carbon export flux was  
554 between  $0.004 \pm 0.002$  (C<sub>soft(AOU)</sub>) and  $0.006 \pm 0.002$  GtC yr<sup>-1</sup> (C<sub>soft(NO<sub>3</sub>)</sub>) for the study area. For  
555 comparison, a recent estimate of global export production accounting for both POC and DOC  
556 was  $8.37 \pm 1.57$  GtC yr<sup>-1</sup> (Sulpis et al., 2023), which amounts to  $0.017 \pm 0.003$  GtC yr<sup>-1</sup> when  
557 scaled down to the study area. This suggests that the increase in the BCP that we observed could  
558 represent an increase in the amount of carbon remineralised by 23% to 35% each year. However,  
559 if the study region is a biological “hotspot” with high baseline productivity and remineralization,  
560 the global average would be an underestimate for this region, so the 23% to 35% increase is an  
561 upper bound. Regardless of its size as a fraction of the baseline remineralization rate, the  
562 magnitude of the DIC increase associated with the BCP is of the same order of magnitude as the  
563 anthropogenic increase in DIC (Fig. 3d and Fig. 4). Thus, while changes in the biological carbon  
564 pump are often considered less significant than anthropogenic CO<sub>2</sub> uptake, they should still be  
565 considered in global carbon budgets.

### 566 4.3.3 Anthropogenic Influence and CO<sub>2</sub> Dynamics

567 Since the early 1960s, the primary driver behind the long-term trend in the ocean carbon sink has  
568 been the rising uptake of anthropogenic CO<sub>2</sub> (Gruber et al., 2023). From 2004 through to 2019,  
569 the global oceanic DIC pool increased at an average rate of  $3.2 \pm 0.7 \text{ Pg C yr}^{-1}$ , with no  
570 statistically detectable difference between the total DIC change and Canth accumulation between  
571 2004 and 2020 (Keppeler et al., 2023). This implies no global net change in  $C_{\text{soft}}$  but does not rule  
572 out a spatial redistribution, driven by various factors including ocean warming, alterations in  
573 marine biology, and other physical changes within the oceans, as discussed above for 40°S.  
574 Thus, our study may be an example of this redistribution effect—as also witnessed in the  
575 northeast Atlantic Ocean (Humphreys et al., 2016). The role of the biological carbon pump  
576 relative to anthropogenic CO<sub>2</sub> uptake in the changing marine DIC pool may be more important  
577 than previously thought.

## 578 5 Conclusions

579 At 40°S in the Atlantic Ocean, from 1972 to 2023, DIC increased, down to approximately 2000  
580 m ( $\gamma_n \approx 27.9 \text{ kg m}^{-3}$ ), with a near-surface maximum rate of  $1.52 \pm 0.11 \mu\text{mol kg}^{-1} \text{ yr}^{-1}$ . Although  
581 at least half of this change can be attributed to anthropogenic CO<sub>2</sub> accumulation, the  
582 intensification of the BCP in this region is evident, with contributions ranging from  $0.20 \pm 0.03$   
583  $\mu\text{mol kg}^{-1} \text{ yr}^{-1}$  to  $0.85 \pm 0.07 \mu\text{mol kg}^{-1} \text{ yr}^{-1}$  (using  $C_{\text{soft(AOU)}}$  and  $C_{\text{soft(NO}_3)}$ , respectively). While  
584 we cannot definitively select one soft tissue pump estimation over another due to inherent  
585 uncertainties in the influence of different processes, the concurrent increase in both  $C_{\text{soft(AOU)}}$  and  
586  $C_{\text{soft(NO}_3)}$  estimates serves as a robust indicator of the intensifying nature of the BCP at this  
587 location amidst various influencing factors.

588  
589 This study at 40°S in the Southern Ocean has also provided valuable insights into the complex  
590 interplay of physical, biological, and anthropogenic factors influencing the dynamics of the BCP.  
591 Our investigation reveals that changes in sea ice dynamics, ocean stratification, wind patterns,  
592 and biological activity, including photosynthesis and organic matter degradation, could all have  
593 played a role in the observed changes in efficiency of the BCP.

594  
595 These findings also highlight the implications of these changes for CO<sub>2</sub> sink behavior and carbon  
596 export. The observed increase in pCO<sub>2</sub> at 40°S and the depth-integrated increase in organic  
597 carbon export flux imply shifts in the region's role in the global carbon cycle. These shifts are not  
598 only vital for understanding the evolution of atmospheric CO<sub>2</sub> concentration but also for  
599 potential future climate change mitigation efforts.

600  
601 Finally, the study addresses anthropogenic influence on CO<sub>2</sub> dynamics. The increasing uptake of  
602 anthropogenic CO<sub>2</sub> and its interplay with the biological carbon pump indicate that the role of the  
603 BCP in DIC changes might be more intricate and significant than previously assumed. This  
604 highlights the need for comprehensive consideration of the biological carbon pump in global  
605 carbon budgets and climate models.

## 606 Supplement

607 The supplement related to this article is available online at: <https://doi.org/>

608

609 **Author contributions**

610 LD and MPH conceptualized the project. LD and MPH curated the data. LD, MPH and OS  
611 performed the investigation. LD conceptualized the methodology, used the necessary software,  
612 visualized the data and prepared the original draft of the paper. LD, MPH, OS and GJR reviewed  
613 and edited the paper.

614

615 **Competing interests**

616 The contact author has declared that neither they nor their co-authors have any competing  
617 interests.

618 **Acknowledgments**

619 We would like to express our sincere gratitude to the Global Ocean Data Analysis Project  
620 (GLODAP) for providing invaluable oceanographic data, which significantly enhanced the  
621 quality and depth of our research. The comprehensive dataset offered by GLODAP played a  
622 pivotal role in this study. We also extend our appreciation to the BGC-Argo program for the  
623 deployment of biogeochemical Argo floats. The data collected by BGC-Argo floats were  
624 instrumental in updating our dataset with recent trends. Finally, we would like to acknowledge  
625 our colleagues and research team for their dedication and hard work throughout this project. This  
626 paper would not have been possible without the collective contributions of these individuals and  
627 organizations. Any errors or omissions remain our own. LD also wishes to thank the Institut de la  
628 mer de Villefranche (France) and in particular the OMTAB team for hosting her during the later  
629 stage of this research project.

630

631 **Open Research Data Availability Statement**

632 All data and code used in this analysis will be available in the GitHub repository at  
633 <https://github.com/louisedelaigue/changing-BCP-40S> by the time of publication. PyCO2SYS  
634 v1.8.1 (Humphreys et al., 2022) was used to solve for the carbonate system, with software  
635 available at <https://doi.org/10.5281/zenodo.3744275> (Humphreys et al., 2024). The Gibbs-  
636 SeaWater (GSW) Oceanographic Toolbox was used to calculate neutral density, with software  
637 available at <https://www.teos-10.org/>. Figures were made with Python version 3.9 (van Rossum  
638 & Drake Jr, 2009).

639 **References**

- 640 Anderson, L. A., & Sarmiento, J. L. (1994). Redfield ratios of remineralization determined by nutrient data analysis.  
641 *Global Biogeochemical Cycles*, 8(1), 65-80. <https://doi.org/10.1029/93gb03318>
- 642 Arrigo, K. R., Robinson, D. H., Worthen, D. L., Dunbar, R. B., DiTullio, G. R., VanWoert, M., & Lizotte, M. P.  
643 (1999). Phytoplankton Community Structure and the Drawdown of Nutrients and CO<sub>2</sub> in the  
644 Southern Ocean. *Science*, 283(5400), 365-367. <https://doi.org/doi:10.1126/science.283.5400.365>
- 645 Arrigo, K. R., van Dijken, G. L., & Strong, A. L. (2015). Environmental controls of marine productivity hot spots  
646 around Antarctica. *Journal of Geophysical Research: Oceans*, 120(8), 5545-5565.  
647 <https://doi.org/10.1002/2015JC010888>
- 648 10.1002/2015JC010888</p>
- 649 Arroyo, M. C., Fassbender, A. J., Carter, B. R., Edwards, C. A., Fiechter, J., Norgaard, A., & Feely, R. A. (2022).  
650 Dissimilar Sensitivities of Ocean Acidification Metrics to Anthropogenic Carbon Accumulation in the  
651 Central North Pacific Ocean and California Current Large Marine Ecosystem. *Geophysical Research*  
652 *Letters*, 49(15), e2022GL097835. <https://doi.org/https://doi.org/10.1029/2022GL097835>

- 653 Ayo, B., Abad, N., Artolozaga, I., Azua, I., Baña, Z., Unanue, M., Gasol, J. M., Duarte, C. M., & Iriberry, J. (2017).  
654 Imbalanced nutrient recycling in a warmer ocean driven by differential response of extracellular enzymatic  
655 activities. *Global Change Biology*, 23(10), 4084-4093. <https://doi.org/https://doi.org/10.1111/gcb.13779>
- 656 Behrenfeld, M. J., O'Malley, R. T., Siegel, D. A., McClain, C. R., Sarmiento, J. L., Feldman, G. C., Milligan, A. J.,  
657 Falkowski, P. G., Letelier, R. M., & Boss, E. S. (2006). Climate-driven trends in contemporary ocean  
658 productivity. *Nature*, 444(7120), 752-755. <https://doi.org/10.1038/nature05317>
- 659 Bittig, H. C., Maurer, T. L., Plant, J. N., Schmechtig, C., Wong, A. P. S., Claustre, H., Trull, T. W., Udaya Bhaskar,  
660 T. V. S., Boss, E., Dall'Olmo, G., Organelli, E., Poteau, A., Johnson, K. S., Hanstein, C., Leymarie, E., Le  
661 Reste, S., Riser, S. C., Rupan, A. R., Taillandier, V., . . . Xing, X. (2019). A BGC-Argo Guide: Planning,  
662 Deployment, Data Handling and Usage [Review]. *Frontiers in Marine Science*, 6.  
663 <https://doi.org/10.3389/fmars.2019.00502>
- 664 Boyd, P. W., & Trull, T. W. (2007). Understanding the export of biogenic particles in oceanic waters: Is there  
665 consensus? *Progress in Oceanography*, 72(4), 276-312.  
666 <https://doi.org/https://doi.org/10.1016/j.pocean.2006.10.007>
- 667 Browning, T. J., Bouman, H. A., Moore, C. M., Schlosser, C., Tarran, G. A., Woodward, E. M. S., & Henderson, G.  
668 M. (2014). Nutrient regimes control phytoplankton ecophysiology in the South Atlantic. *Biogeosciences*,  
669 11(2), 463-479. <https://doi.org/10.5194/bg-11-463-2014>
- 670 Buesseler, K. O., Antia, A. N., Chen, M., Fowler, S. W., Gardner, W. D., Gustafsson, O., Harada, K., Michaels, A.  
671 F., Rutgers van der Loeff, M., & Sarin, M. (2007). An assessment of the use of sediment traps for  
672 estimating upper ocean particle fluxes. *Journal of marine research*, 65(3), 345-416.
- 673 Cael, B. B., Dutkiewicz, S., & Henson, S. (2021). Abrupt shifts in 21st-century plankton communities. *Science*  
674 *Advances*, 7(44), eabf8593. <https://doi.org/doi:10.1126/sciadv.abf8593>
- 675 Chen, C.-T. A. (1978). Decomposition of Calcium Carbonate and Organic Carbon in the Deep Oceans. *Science*,  
676 201(4357), 735-736. <https://doi.org/doi:10.1126/science.201.4357.735>
- 677 Chen, J., & Thornton, D. C. (2015). Transparent exopolymer particle production and aggregation by a marine  
678 planktonic diatom (*Thalassiosira weissflogii*) at different growth rates. *J Phycol*, 51(2), 381-393.  
679 <https://doi.org/10.1111/jpy.12285>
- 680 Council, N. R. (2010). *Ocean Acidification: A National Strategy to Meet the Challenges of a Changing Ocean*. The  
681 National Academies Press. <https://doi.org/doi:10.17226/12904>
- 682 Davila, X., Gebbie, G., Brakstad, A., Lauvset, S. K., McDonagh, E. L., Schwinger, J., & Olsen, A. (2022). How Is  
683 the Ocean Anthropogenic Carbon Reservoir Filled? *Global Biogeochemical Cycles*, 36(5),  
684 e2021GB007055. <https://doi.org/https://doi.org/10.1029/2021GB007055>
- 685 De Jong, J., Schoemann, V., Lannuzel, D., Croot, P., de Baar, H., & Tison, J. L. (2012). Natural iron fertilization of  
686 the Atlantic sector of the Southern Ocean by continental shelf sources of the Antarctic Peninsula. *Journal*  
687 *of Geophysical Research: Biogeosciences*, 117(G1).
- 688 De La Rocha, C. L., & Passow, U. (2014). 8.4 - The Biological Pump. In H. D. Holland & K. K. Turekian (Eds.),  
689 *Treatise on Geochemistry (Second Edition)* (pp. 93-122). Elsevier.  
690 <https://doi.org/https://doi.org/10.1016/B978-0-08-095975-7.00604-5>
- 691 DeVries, T. (2018). New directions for ocean nutrients. *Nature Geoscience*, 11(1), 15-16.  
692 <https://doi.org/10.1038/s41561-017-0042-z>
- 693 DeVries, T., Holzer, M., & Primeau, F. (2017). Recent increase in oceanic carbon uptake driven by weaker upper-  
694 ocean overturning. *Nature*, 542(7640), 215-218. <https://doi.org/10.1038/nature21068>
- 695 Dickson, A. G. (1990). Standard potential of the reaction:  $\text{AgCl(s)} + 12\text{H}_2\text{(g)} = \text{Ag(s)} + \text{HCl(aq)}$ , and and the  
696 standard acidity constant of the ion  $\text{HSO}_4^-$  in synthetic sea water from 273.15 to 318.15 K. *The Journal of*  
697 *Chemical Thermodynamics*, 22(2), 113-127. [https://doi.org/https://doi.org/10.1016/0021-9614\(90\)90074-Z](https://doi.org/https://doi.org/10.1016/0021-9614(90)90074-Z)
- 698 Dickson, A. G. (1992). *The determination of total dissolved inorganic carbon in sea water using*  
699 *extraction/coulometry: The first stage of a collaborative study*. <https://www.osti.gov/biblio/5823722>
- 700 Dickson, A. G., & Riley, J. P. (1979). The estimation of acid dissociation constants in sea-water media from  
701 potentiometric titrations with strong base. II. The dissociation of phosphoric acid. *Marine Chemistry*, 7(2),  
702 101-109. [https://doi.org/https://doi.org/10.1016/0304-4203\(79\)90002-1](https://doi.org/https://doi.org/10.1016/0304-4203(79)90002-1)
- 703 England, M. H., McGregor, S., Spence, P., Meehl, G. A., Timmermann, A., Cai, W., Gupta, A. S., McPhaden, M. J.,  
704 Purich, A., & Santoso, A. (2014). Recent intensification of wind-driven circulation in the Pacific and the  
705 ongoing warming hiatus. *Nature Climate Change*, 4(3), 222-227. <https://doi.org/10.1038/nclimate2106>
- 706 Feely, R. A., Sabine, C. L., Lee, K., Berelson, W., Kleypas, J., Fabry, V. J., & Millero, F. J. (2004). Impact of  
707 anthropogenic  $\text{CO}_2$  on the  $\text{CaCO}_3$  system in the oceans. *Science*, 305(5682), 362-366.

- 708 Figuerola, B., Hancock, A. M., Bax, N., Cummings, V. J., Downey, R., Griffiths, H. J., Smith, J., & Stark, J. S.  
 709 (2021). A Review and Meta-Analysis of Potential Impacts of Ocean Acidification on Marine Calcifiers  
 710 From the Southern Ocean [Review]. *Frontiers in Marine Science*, 8.  
 711 <https://doi.org/10.3389/fmars.2021.584445>
- 712 Fine, R. A., Peacock, S., Maltrud, M. E., & Bryan, F. O. (2017). A new look at ocean ventilation time scales and  
 713 their uncertainties. *Journal of Geophysical Research: Oceans*, 122(5), 3771-3798.  
 714 <https://doi.org/https://doi.org/10.1002/2016JC012529>
- 715 Fontela, M., Velo, A., Gilcoto, M., & Pérez, F. F. (2021). Anthropogenic CO<sub>2</sub> and ocean acidification in  
 716 Argentine Basin Water Masses over almost five decades of observations. *Sci Total Environ*, 779, 146570.  
 717 <https://doi.org/10.1016/j.scitotenv.2021.146570>
- 718 Friedlingstein, P., O'Sullivan, M., Jones, M. W., Andrew, R. M., Bakker, D. C. E., Hauck, J., Landschützer, P., Le  
 719 Quéré, C., Luijkx, I. T., Peters, G. P., Peters, W., Pongratz, J., Schwingshackl, C., Sitch, S., Canadell, J. G.,  
 720 Ciais, P., Jackson, R. B., Alin, S. R., Anthoni, P., . . . Zheng, B. (2023). Global Carbon Budget 2023. *Earth*  
 721 *Syst. Sci. Data*, 15(12), 5301-5369. <https://doi.org/10.5194/essd-15-5301-2023>
- 722 Fritsch, F. N., & Carlson, R. E. (1980). Monotone Piecewise Cubic Interpolation. *SIAM Journal on Numerical*  
 723 *Analysis*, 17(2), 238-246. <https://doi.org/10.1137/0717021>
- 724 Garcia-Soto, C., Cheng, L., Caesar, L., Schmidtko, S., Jewett, E. B., Cheripka, A., Rigor, I., Caballero, A., Chiba,  
 725 S., Báez, J. C., Zielinski, T., & Abraham, J. P. (2021). An Overview of Ocean Climate Change Indicators:  
 726 Sea Surface Temperature, Ocean Heat Content, Ocean pH, Dissolved Oxygen Concentration, Arctic Sea  
 727 Ice Extent, Thickness and Volume, Sea Level and Strength of the AMOC (Atlantic Meridional Overturning  
 728 Circulation) [Review]. *Frontiers in Marine Science*, 8. <https://doi.org/10.3389/fmars.2021.642372>
- 729 Garcia, H. E., & Gordon, L. I. (1992). Oxygen solubility in seawater: Better fitting equations. *Limnology and*  
 730 *Oceanography*, 37(6), 1307-1312. <https://doi.org/https://doi.org/10.4319/lo.1992.37.6.1307>
- 731 Gjelstrup, C. V. B., Sejr, M. K., de Steur, L., Christiansen, J. S., Granskog, M. A., Koch, B. P., Møller, E. F.,  
 732 Winding, M. H. S., & Stedmon, C. A. (2022). Vertical redistribution of principle water masses on the  
 733 Northeast Greenland Shelf. *Nature Communications*, 13(1), 7660. <https://doi.org/10.1038/s41467-022-35413-z>
- 734
- 735 Groeskamp, S., Lenton, A., Matear, R., Sloyan, B. M., & Langlais, C. (2016). Anthropogenic carbon in the ocean—  
 736 Surface to interior connections. *Global Biogeochemical Cycles*, 30(11), 1682-1698.  
 737 <https://doi.org/https://doi.org/10.1002/2016GB005476>
- 738 Gruber, N., Bakker, D. C. E., DeVries, T., Gregor, L., Hauck, J., Landschützer, P., McKinley, G. A., & Müller, J. D.  
 739 (2023). Trends and variability in the ocean carbon sink. *Nature Reviews Earth & Environment*, 4(2), 119-  
 740 134. <https://doi.org/10.1038/s43017-022-00381-x>
- 741 Gruber, N., Clement, D., Carter, B. R., Feely, R. A., van Heuven, S., Hoppema, M., Ishii, M., Key, R. M., Kozyr,  
 742 A., Lauvset, S. K., Lo Monaco, C., Mathis, J. T., Murata, A., Olsen, A., Perez, F. F., Sabine, C. L., Tanhua,  
 743 T., & Wanninkhof, R. (2019). The oceanic sink for anthropogenic CO<sub>2</sub> from 1994 to 2007. *Science*,  
 744 363(6432), 1193-1199. <https://doi.org/10.1126/science.aau5153>
- 745 Gruber, N., Sarmiento, J., Robinson, A., McCarthy, J., & Rothschild, B. (2002). The Sea: Ideas and Observations on  
 746 Progress in the Study of the Seas. In: Wiley New York.
- 747 Gruber, N., Sarmiento, J. L., & Stocker, T. F. (1996). An improved method for detecting anthropogenic CO<sub>2</sub> in the  
 748 oceans. *Global Biogeochemical Cycles*, 10(4), 809-837. <https://doi.org/10.1029/96gb01608>
- 749 Heinze, C., Maier-Reimer, E., & Winn, K. (1991). Glacial pCO<sub>2</sub> Reduction by the World Ocean: Experiments With  
 750 the Hamburg Carbon Cycle Model. *Paleoceanography*, 6(4), 395-430.  
 751 <https://doi.org/https://doi.org/10.1029/91PA00489>
- 752 Henley, S. F., Cavan, E. L., Fawcett, S. E., Kerr, R., Monteiro, T., Sherrell, R. M., Bowie, A. R., Boyd, P. W.,  
 753 Barnes, D. K. A., Schloss, I. R., Marshall, T., Flynn, R., & Smith, S. (2020). Changing Biogeochemistry of  
 754 the Southern Ocean and Its Ecosystem Implications [Original Research]. *Frontiers in Marine Science*, 7.  
 755 <https://doi.org/10.3389/fmars.2020.00581>
- 756 Henson, S. A., Laufkötter, C., Leung, S., Giering, S. L. C., Palevsky, H. I., & Cavan, E. L. (2022). Uncertain  
 757 response of ocean biological carbon export in a changing world. *Nature Geoscience*, 15(4), 248-254.  
 758 <https://doi.org/10.1038/s41561-022-00927-0>
- 759 Henson, S. A., Sanders, R., & Madsen, E. (2012). Global patterns in efficiency of particulate organic carbon export  
 760 and transfer to the deep ocean. *Global Biogeochemical Cycles*, 26(1).
- 761 Hofmann, A. F., Peltzer, E. T., Walz, P. M., & Brewer, P. G. (2011). Hypoxia by degrees: Establishing definitions  
 762 for a changing ocean. *Deep Sea Research Part I: Oceanographic Research Papers*, 58(12), 1212-1226.  
 763 <https://doi.org/https://doi.org/10.1016/j.dsr.2011.09.004>

- 764 Humphreys, M. P., Griffiths, A. M., Achterberg, E. P., Holliday, N. P., Rérolle, V. M., Menzel Barraqueta, J. L.,  
765 Couldrey, M. P., Oliver, K. I., Hartman, S. E., & Esposito, M. (2016). Multidecadal accumulation of  
766 anthropogenic and remineralized dissolved inorganic carbon along the Extended Ellett Line in the northeast  
767 Atlantic Ocean. *Global Biogeochemical Cycles*, *30*(2), 293-310.
- 768 Humphreys, M. P., Lewis, E. R., Sharp, J. D., & Pierrot, D. (2022). PyCO2SYS v1.8: marine carbonate system  
769 calculations in Python. *Geosci. Model Dev.*, *15*(1), 15-43. <https://doi.org/10.5194/gmd-15-15-2022>
- 770 Humphreys, M. P., Schiller, A. J., Sandborn, D., Gregor, L., Pierrot, D., van Heuven, S. M. A. C., Lewis, E. R., &  
771 Wallace, D. W. R. (2024). PyCO2SYS: marine carbonate system calculations in Python (v1.8.3). Zenodo.  
772 <https://doi.org/10.5281/zenodo.10671397>
- 773 Inomura, K., Deutsch, C., Jahn, O., Dutkiewicz, S., & Follows, M. J. (2022). Global patterns in marine organic  
774 matter stoichiometry driven by phytoplankton ecophysiology. *Nature Geoscience*, *15*(12), 1034-1040.  
775 <https://doi.org/10.1038/s41561-022-01066-2>
- 776 Ito, T., & Follows, M. J. (2005). Preformed phosphate, soft tissue pump and atmospheric CO<sub>2</sub>. *Journal of marine  
777 research*, *63*(4), 813-839.
- 778 Johnson, K. S., Mazloff, M. R., Bif, M. B., Takeshita, Y., Jannasch, H. W., Maurer, T. L., Plant, J. N., Verdy, A.,  
779 Walz, P. M., Riser, S. C., & Talley, L. D. (2022). Carbon to Nitrogen Uptake Ratios Observed Across the  
780 Southern Ocean by the SOCCOM Profiling Float Array. *Journal of Geophysical Research: Oceans*, *127*(9),  
781 e2022JC018859. <https://doi.org/https://doi.org/10.1029/2022JC018859>
- 782 Keppler, L., & Landschützer, P. (2019). Regional Wind Variability Modulates the Southern Ocean Carbon Sink.  
783 *Scientific reports*, *9*(1), 7384. <https://doi.org/10.1038/s41598-019-43826-y>
- 784 Keppler, L., Landschützer, P., Lauvset, S. K., & Gruber, N. (2023). Recent Trends and Variability in the Oceanic  
785 Storage of Dissolved Inorganic Carbon. *Global Biogeochemical Cycles*, *37*(5), e2022GB007677.  
786 <https://doi.org/https://doi.org/10.1029/2022GB007677>
- 787 Khatiwala, S., Primeau, F., & Hall, T. (2009). Reconstruction of the history of anthropogenic CO<sub>2</sub> concentrations in  
788 the ocean. *Nature*, *462*(7271), 346-349. <https://doi.org/10.1038/nature08526>
- 789 Khatiwala, S., Tanhua, T., Mikaloff Fletcher, S., Gerber, M., Doney, S. C., Graven, H. D., Gruber, N., McKinley, G.  
790 A., Murata, A., Ríos, A. F., & Sabine, C. L. (2013). Global ocean storage of anthropogenic carbon.  
791 *Biogeosciences*, *10*(4), 2169-2191. <https://doi.org/10.5194/bg-10-2169-2013>
- 792 Kim, H.-J., Kim, H. J., Yang, E.-J., Cho, K.-H., Jung, J., Kang, S.-H., Lee, K.-E., Cho, S., Kim, D., & , o. b. o. t. C.  
793 W. G. (2021). Temporal and Spatial Variations in Particle Fluxes on the Chukchi Sea and East Siberian Sea  
794 Slopes From 2017 to 2018 [Original Research]. *Frontiers in Marine Science*, *7*.  
795 <https://doi.org/10.3389/fmars.2020.609748>
- 796 Landschützer, P., Gruber, N., Haumann, F. A., Rödenbeck, C., Bakker, D. C. E., van Heuven, S., Hoppema, M.,  
797 Metzl, N., Sweeney, C., Takahashi, T., Tilbrook, B., & Wanninkhof, R. (2015). The reinvigoration of the  
798 Southern Ocean carbon sink. *Science*, *349*(6253), 1221-1224. <https://doi.org/doi:10.1126/science.aab2620>
- 799 Lannuzel, D., Schoemann, V., De Jong, J., Pasquer, B., Van der Merwe, P., Masson, F., Tison, J. L., & Bowie, A.  
800 (2010). Distribution of dissolved iron in Antarctic sea ice: Spatial, seasonal, and inter-annual variability.  
801 *Journal of Geophysical Research: Biogeosciences*, *115*(G3).
- 802 Lannuzel, D., Vancoppenolle, M., Van der Merwe, P., De Jong, J., Meiners, K. M., Grotti, M., Nishioka, J., &  
803 Schoemann, V. (2016). Iron in sea ice: Review and new insights. *Elem Sci Anth*, *4*.
- 804 Laufkötter, C., Vogt, M., Gruber, N., Aumont, O., Bopp, L., Doney, S. C., Dunne, J. P., Hauck, J., John, J. G., &  
805 Lima, I. D. (2016). Projected decreases in future marine export production: the role of the carbon flux  
806 through the upper ocean ecosystem. *Biogeosciences*, *13*(13), 4023-4047.
- 807 Lauvset, S. K., Lange, N., Tanhua, T., Bittig, H. C., Olsen, A., Kozyr, A., Alin, S., Álvarez, M., Azetsu-Scott, K., &  
808 Barbero, L. (2022). GLODAPv2. 2022: the latest version of the global interior ocean biogeochemical data  
809 product. *Earth System Science Data*, *14*(12), 5543-5572.
- 810 Lee, K., Tong, L. T., Millero, F. J., Sabine, C. L., Dickson, A. G., Goyet, C., Park, G. H., Wanninkhof, R., Feely, R.  
811 A., & Key, R. M. (2006). Global relationships of total alkalinity with salinity and temperature in surface  
812 waters of the world's oceans. *Geophysical Research Letters*, *33*(19).
- 813 Lencina-Avila, J. M., Ito, R. G., Garcia, C. A. E., & Tavano, V. M. (2016). Sea-air carbon dioxide fluxes along 35°S  
814 in the South Atlantic Ocean. *Deep Sea Research Part I: Oceanographic Research Papers*, *115*, 175-187.  
815 <https://doi.org/https://doi.org/10.1016/j.dsr.2016.06.004>
- 816 Li, G., Cheng, L., Zhu, J., Trenberth, K. E., Mann, M. E., & Abraham, J. P. (2020). Increasing ocean stratification  
817 over the past half-century. *Nature Climate Change*, *10*(12), 1116-1123. [https://doi.org/10.1038/s41558-  
818 020-00918-2](https://doi.org/10.1038/s41558-020-00918-2)

- 819 Liu, Y., Moore, J. K., Primeau, F., & Wang, W. L. (2023). Reduced CO<sub>2</sub> uptake and growing nutrient sequestration  
 820 from slowing overturning circulation. *Nature Climate Change*, 13(1), 83-90.  
 821 <https://doi.org/10.1038/s41558-022-01555-7>
- 822 Marsay, C. M., Sanders, R. J., Henson, S. A., Pabortsava, K., Achterberg, E. P., & Lampitt, R. S. (2015).  
 823 Attenuation of sinking particulate organic carbon flux through the mesopelagic ocean. *Proceedings of the*  
 824 *National Academy of Sciences*, 112(4), 1089-1094.
- 825 Martiny, A. C., Pham, C. T. A., Primeau, F. W., Vrugt, J. A., Moore, J. K., Levin, S. A., & Lomas, M. W. (2013).  
 826 Strong latitudinal patterns in the elemental ratios of marine plankton and organic matter. *Nature*  
 827 *Geoscience*, 6(4), 279-283. <https://doi.org/10.1038/ngeo1757>
- 828 Matsumoto, K., Tanioka, T., & Rickaby, R. (2020). Linkages Between Dynamic Phytoplankton C: N: P and the  
 829 Ocean Carbon Cycle Under Climate Change. *Oceanography*, 33(2).
- 830 McDougall, T. J., & Barker, P. M. (2011). Getting started with TEOS-10 and the Gibbs Seawater (GSW)  
 831 oceanographic toolbox. *SCOR/IAPSO WG*, 127, 1-28.
- 832 Mignot, A., D'Ortenzio, F., Taillandier, V., Cossarini, G., & Salon, S. (2019). Quantifying Observational Errors in  
 833 Biogeochemical-Argo Oxygen, Nitrate, and Chlorophyll a Concentrations. *Geophysical Research Letters*,  
 834 46(8), 4330-4337. <https://doi.org/https://doi.org/10.1029/2018GL080541>
- 835 Moore, J. K., Doney, S. C., Glover, D. M., & Fung, I. Y. (2001). Iron cycling and nutrient-limitation patterns in  
 836 surface waters of the World Ocean. *Deep Sea Research Part II: Topical Studies in Oceanography*, 49(1),  
 837 463-507. [https://doi.org/https://doi.org/10.1016/S0967-0645\(01\)00109-6](https://doi.org/https://doi.org/10.1016/S0967-0645(01)00109-6)
- 838 Morley, S. A., Abele, D., Barnes, D. K. A., Cárdenas, C. A., Cotté, C., Gutt, J., Henley, S. F., Höfer, J., Hughes, K.  
 839 A., Martin, S. M., Moffat, C., Raphael, M., Stammerjohn, S. E., Suckling, C. C., Tulloch, V. J. D., Waller,  
 840 C. L., & Constable, A. J. (2020). Global Drivers on Southern Ocean Ecosystems: Changing Physical  
 841 Environments and Anthropogenic Pressures in an Earth System [Review]. *Frontiers in Marine Science*, 7.  
 842 <https://doi.org/10.3389/fmars.2020.547188>
- 843 Orr, J. C., Fabry, V. J., Aumont, O., Bopp, L., Doney, S. C., Feely, R. A., Gnanadesikan, A., Gruber, N., Ishida, A.,  
 844 Joos, F., Key, R. M., Lindsay, K., Maier-Reimer, E., Matear, R., Monfray, P., Mouchet, A., Najjar, R. G.,  
 845 Plattner, G.-K., Rodgers, K. B., . . . Yool, A. (2005). Anthropogenic ocean acidification over the twenty-  
 846 first century and its impact on calcifying organisms. *Nature*, 437(7059), 681-686.  
 847 <https://doi.org/10.1038/nature04095>
- 848 Padin, X., Vázquez-Rodríguez, M., Castaño, M., Velo, A., Alonso-Pérez, F., Gago, J., Gilcoto, M., Álvarez, M.,  
 849 Pardo, P. C., & de La Paz, M. (2010). Air-Sea CO<sub>2</sub> fluxes in the Atlantic as measured during boreal spring  
 850 and autumn. *Biogeosciences*, 7(5), 1587-1606.
- 851 Passow, U. (2002). Transparent exopolymer particles (TEP) in aquatic environments. *Progress in Oceanography*,  
 852 55(3), 287-333. [https://doi.org/https://doi.org/10.1016/S0079-6611\(02\)00138-6](https://doi.org/https://doi.org/10.1016/S0079-6611(02)00138-6)
- 853 Piñango, A., Kerr, R., Orselli, I. B. M., Carvalho, A. d. C. O., Azar, E., Karstensen, J., & Garcia, C. A. E. (2022).  
 854 Ocean Acidification and Long-Term Changes in the Carbonate System Properties of the South Atlantic  
 855 Ocean. *Global Biogeochemical Cycles*, 36(9), e2021GB007196.  
 856 <https://doi.org/https://doi.org/10.1029/2021GB007196>
- 857 Polovina, J. J., Howell, E. A., & Abecassis, M. (2008). Ocean's least productive waters are expanding. *Geophysical*  
 858 *Research Letters*, 35(3). <https://doi.org/https://doi.org/10.1029/2007GL031745>
- 859 Priest, T., von Appen, W.-J., Oldenburg, E., Popa, O., Torres-Valdés, S., Bienhold, C., Metfies, K., Boulton, W.,  
 860 Mock, T., Fuchs, B. M., Amann, R., Boetius, A., & Wietz, M. (2023). Atlantic water influx and sea-ice  
 861 cover drive taxonomic and functional shifts in Arctic marine bacterial communities. *The ISME Journal*,  
 862 17(10), 1612-1625. <https://doi.org/10.1038/s41396-023-01461-6>
- 863 Redfield, A. C. (1958). The biological control of chemical factors in the environment. *American scientist*, 46(3),  
 864 230A-221.
- 865 Redfield, A. C. (1963). The influence of organisms on the composition of seawater. *The Sea*, 2, 26-77.  
 866 <https://ci.nii.ac.jp/naid/10003517839/en/>
- 867 Riebesell, U., Körtzinger, A., & Oschlies, A. (2009). Sensitivities of marine carbon fluxes to ocean change.  
 868 *Proceedings of the National Academy of Sciences*, 106(49), 20602-20609.  
 869 <https://doi.org/doi:10.1073/pnas.0813291106>
- 870 Sabine, C. L., Feely, R. A., Gruber, N., Key, R. M., Lee, K., Bullister, J. L., Wanninkhof, R., Wong, C. S., Wallace,  
 871 D. W. R., Tilbrook, B., Millero, F. J., Peng, T.-H., Kozyr, A., Ono, T., & Rios, A. F. (2004). The Oceanic  
 872 Sink for Anthropogenic CO<sub>2</sub>. *Science*, 305(5682), 367-371. <https://doi.org/10.1126/science.1097403>
- 873 Sabine, C. L., & Tanhua, T. (2010). Estimation of Anthropogenic CO<sub>2</sub> Inventories in the Ocean. *Annual Review of*  
 874 *Marine Science*, 2(1), 175-198. <https://doi.org/10.1146/annurev-marine-120308-080947>

- 875 Santos, G. C., Kerr, R., Azevedo, J. L. L., Mendes, C. R. B., & da Cunha, L. C. (2016). Influence of Antarctic  
876 Intermediate Water on the deoxygenation of the Atlantic Ocean. *Dynamics of Atmospheres and Oceans*, 76,  
877 72-82. <https://doi.org/https://doi.org/10.1016/j.dynatmoce.2016.09.002>
- 878 Sarmiento, J. L. (2006). *Ocean biogeochemical dynamics*. Princeton university press.
- 879 Sarmiento, J. L., Hughes, T. M. C., Stouffer, R. J., & Manabe, S. (1998). Simulated response of the ocean carbon  
880 cycle to anthropogenic climate warming. *Nature*, 393(6682), 245-249. <https://doi.org/10.1038/30455>
- 881 Sarmiento, J. L., Orr, J. C., & Siegenthaler, U. (1992). A perturbation simulation of CO<sub>2</sub> uptake in an ocean general  
882 circulation model. *Journal of Geophysical Research: Oceans*, 97(C3), 3621-3645.  
883 <https://doi.org/https://doi.org/10.1029/91JC02849>
- 884 Sauzède, R., Claustre, H., Uitz, J., Jamet, C., Dall'Olmo, G., D'Ortenzio, F., Gentili, B., Poteau, A., & Schmechtig,  
885 C. (2016). A neural network-based method for merging ocean color and Argo data to extend surface bio-  
886 optical properties to depth: Retrieval of the particulate backscattering coefficient. *Journal of Geophysical*  
887 *Research: Oceans*, 121(4), 2552-2571. <https://doi.org/https://doi.org/10.1002/2015JC011408>
- 888 Schlunegger, S., Rodgers, K. B., Sarmiento, J. L., Frölicher, T. L., Dunne, J. P., Ishii, M., & Slater, R. (2019).  
889 Emergence of anthropogenic signals in the ocean carbon cycle. *Nature Climate Change*, 9(9), 719-725.  
890 <https://doi.org/10.1038/s41558-019-0553-2>
- 891 Schmidtko, S., Stramma, L., & Visbeck, M. (2017). Decline in global oceanic oxygen content during the past five  
892 decades. *Nature*, 542(7641), 335-339. <https://doi.org/10.1038/nature21399>
- 893 Soppa, M. A., Völker, C., & Bracher, A. (2016). Diatom Phenology in the Southern Ocean: Mean Patterns, Trends  
894 and the Role of Climate Oscillations. *Remote Sensing*, 8(5), 420. [https://www.mdpi.com/2072-](https://www.mdpi.com/2072-4292/8/5/420)  
895 [4292/8/5/420](https://www.mdpi.com/2072-4292/8/5/420)
- 896 Sulpis, O., Lauvset, S. K., & Hagens, M. (2020). Current estimates of K1\* and K2\* appear inconsistent with  
897 measured CO<sub>2</sub> system parameters in cold oceanic regions. *Ocean Sci.*, 16(4), 847-862.  
898 <https://doi.org/10.5194/os-16-847-2020>
- 899 Sulpis, O., Trossman, D. S., Holzer, M., Jeansson, E., Lauvset, S. K., & Middelburg, J. J. (2023). Respiration  
900 Patterns in the Dark Ocean. *Global Biogeochemical Cycles*, 37(8), e2023GB007747.  
901 <https://doi.org/https://doi.org/10.1029/2023GB007747>
- 902 Szewczyk, C. J., Smith, E. M., & Benitez-Nelson, C. R. (2023). Temperature sensitivity of oxygen demand varies as  
903 a function of organic matter source [Original Research]. *Frontiers in Marine Science*, 10.  
904 <https://doi.org/10.3389/fmars.2023.1133336>
- 905 Tagliabue, A., Sallée, J.-B., Bowie, A. R., Lévy, M., Swart, S., & Boyd, P. W. (2014). Surface-water iron supplies in  
906 the Southern Ocean sustained by deep winter mixing. *Nature Geoscience*, 7(4), 314-320.  
907 <https://doi.org/10.1038/ngeo2101>
- 908 Takahashi, T., Feely, R. A., Weiss, R. F., Wanninkhof, R. H., Chipman, D. W., Sutherland, S. C., & Takahashi, T.  
909 T. (1997). Global air-sea flux of CO<sub>2</sub>: An estimate based on measurements of sea-air pCO<sub>2</sub> difference.  
910 *Proceedings of the National Academy of Sciences*, 94(16), 8292-8299.
- 911 Takahashi, T., Sutherland, S. C., Sweeney, C., Poisson, A., Metz, N., Tilbrook, B., Bates, N., Wanninkhof, R.,  
912 Feely, R. A., Sabine, C., Olafsson, J., & Nojiri, Y. (2002). Global sea-air CO<sub>2</sub> flux based on climatological  
913 surface ocean pCO<sub>2</sub>, and seasonal biological and temperature effects. *Deep Sea Research Part II: Topical*  
914 *Studies in Oceanography*, 49(9-10), 1601-1622. [https://doi.org/10.1016/S0967-0645\(02\)00003-6](https://doi.org/10.1016/S0967-0645(02)00003-6)
- 915 Tanhua, T., Hoppema, M., Jones, E. M., Stöven, T., Hauck, J., Dávila, M. G., Santana-Casiano, M., Álvarez, M., &  
916 Strass, V. H. (2017). Temporal changes in ventilation and the carbonate system in the Atlantic sector of the  
917 Southern Ocean. *Deep Sea Research Part II: Topical Studies in Oceanography*, 138, 26-38.  
918 <https://doi.org/https://doi.org/10.1016/j.dsr2.2016.10.004>
- 919 Tanioka, T., & Matsumoto, K. (2020). A meta-analysis on environmental drivers of marine phytoplankton  
920 C&thinsp;:&thinsp;N&thinsp;:&thinsp;P. *Biogeosciences*, 17(11), 2939-2954. [https://doi.org/10.5194/bg-](https://doi.org/10.5194/bg-17-2939-2020)  
921 [17-2939-2020](https://doi.org/10.5194/bg-17-2939-2020)
- 922 Tian, H.-A., van Manen, M., Bunnell, Z. B., Jung, J., Lee, S. H., Kim, T.-W., Reichart, G.-J., Conway, T. M., &  
923 Middag, R. (2023). Biogeochemistry of iron in coastal Antarctica: isotopic insights for external sources and  
924 biological uptake in the Amundsen Sea polynyas. *Geochimica et Cosmochimica Acta*, 363, 51-67.  
925 <https://doi.org/https://doi.org/10.1016/j.gca.2023.10.029>
- 926 Toggweiler, J., Gnanadesikan, A., Carson, S., Murnane, R., & Sarmiento, J. L. (2003). Representation of the carbon  
927 cycle in box models and GCMs: 1. Solubility pump. *Global Biogeochemical Cycles*, 17(1).
- 928 Toseland, A., Daines, S. J., Clark, J. R., Kirkham, A., Strauss, J., Uhlig, C., Lenton, T. M., Valentin, K., Pearson, G.  
929 A., Moulton, V., & Mock, T. (2013). The impact of temperature on marine phytoplankton resource  
930 allocation and metabolism. *Nature Climate Change*, 3(11), 979-984. <https://doi.org/10.1038/nclimate1989>

- 931 Toullec, J., & Moriceau, B. (2018). Transparent Exopolymeric Particles (TEP) Selectively Increase Biogenic Silica  
932 Dissolution From Fossil Diatoms as Compared to Fresh Diatoms [Original Research]. *Frontiers in Marine*  
933 *Science*, 5. <https://doi.org/10.3389/fmars.2018.00102>
- 934 Uppström, L. R. (1974). The boron/chlorinity ratio of deep-sea water from the Pacific Ocean. *Deep Sea Research*  
935 *and Oceanographic Abstracts*, 21(2), 161-162. [https://doi.org/https://doi.org/10.1016/0011-7471\(74\)90074-](https://doi.org/https://doi.org/10.1016/0011-7471(74)90074-6)  
936 [6](https://doi.org/https://doi.org/10.1016/0011-7471(74)90074-6)
- 937 van de Waal, D. B., Verschoor, A. M., Verspagen, J. M., van Donk, E., & Huisman, J. (2010). Climate-driven  
938 changes in the ecological stoichiometry of aquatic ecosystems. *Frontiers in Ecology and the Environment*,  
939 8(3), 145-152. <https://doi.org/https://doi.org/10.1890/080178>
- 940 Van Rossum, G., & Drake Jr, F. L. (2009). Python 3 reference manual. Software.
- 941 Virtanen, P., Gommers, R., Oliphant, T. E., Haberland, M., Reddy, T., Cournapeau, D., Burovski, E., Peterson, P.,  
942 Weckesser, W., Bright, J., van der Walt, S. J., Brett, M., Wilson, J., Millman, K. J., Mayorov, N., Nelson,  
943 A. R. J., Jones, E., Kern, R., Larson, E., . . . SciPy, C. (2020). SciPy 1.0: fundamental algorithms for  
944 scientific computing in Python. *Nature Methods*, 17(3), 261-272. [https://doi.org/10.1038/s41592-019-0686-](https://doi.org/10.1038/s41592-019-0686-2)  
945 [2](https://doi.org/10.1038/s41592-019-0686-2)
- 946 Volk, T., & Hoffert, M. I. (1985). Ocean Carbon Pumps: Analysis of Relative Strengths and Efficiencies in Ocean-  
947 Driven Atmospheric CO<sub>2</sub> Changes. In *The carbon cycle and atmospheric CO<sub>2</sub>: Natural variations*  
948 *Archean to present* (pp. 99-110). <https://doi.org/10.1029/GM032p0099>
- 949 von Appen, W.-J., Waite, A. M., Bergmann, M., Bienhold, C., Boebel, O., Bracher, A., Cisewski, B., Hagemann, J.,  
950 Hoppema, M., Iversen, M. H., Konrad, C., Krumpfen, T., Lochthofen, N., Metfies, K., Niehoff, B., Nöthig,  
951 E.-M., Purser, A., Salter, I., Schaber, M., . . . Boetius, A. (2021). Sea-ice derived meltwater stratification  
952 slows the biological carbon pump: results from continuous observations. *Nature Communications*, 12(1),  
953 7309. <https://doi.org/10.1038/s41467-021-26943-z>
- 954 Wanninkhof, R. (2014). Relationship between wind speed and gas exchange over the ocean revisited. *Limnology*  
955 *and Oceanography: Methods*, 12(6), 351-362. <https://doi.org/10.4319/lom.2014.12.351>
- 956 Waugh, D. W., Primeau, F., DeVries, T., & Holzer, M. (2013). Recent Changes in the Ventilation of the Southern  
957 Oceans. *Science*, 339(6119), 568-570. <https://doi.org/doi:10.1126/science.1225411>
- 958 Wei, J., Gunn, K. L., & Reece, R. (2022). Mid-Ocean Ridge and Storm Enhanced Mixing in the Central South  
959 Atlantic Thermocline [Original Research]. *Frontiers in Marine Science*, 8.  
960 <https://doi.org/10.3389/fmars.2021.771973>
- 961 Williams, N. L., Juranek, L. W., Feely, R. A., Johnson, K. S., Sarmiento, J. L., Talley, L. D., Dickson, A. G., Gray,  
962 A. R., Wanninkhof, R., Russell, J. L., Riser, S. C., & Takeshita, Y. (2017). Calculating surface ocean pCO<sub>2</sub>  
963 from biogeochemical Argo floats equipped with pH: An uncertainty analysis. *Global Biogeochemical*  
964 *Cycles*, 31(3), 591-604. <https://doi.org/https://doi.org/10.1002/2016GB005541>
- 965 Wolf-Gladrow, D. A., Zeebe, R. E., Klaas, C., Körtzinger, A., & Dickson, A. G. (2007). Total alkalinity: The  
966 explicit conservative expression and its application to biogeochemical processes. *Marine Chemistry*, 106(1-  
967 2), 287-300.
- 968 Yvon-Durocher, G., Schaum, C.-E., & Trimmer, M. (2017). The Temperature Dependence of Phytoplankton  
969 Stoichiometry: Investigating the Roles of Species Sorting and Local Adaptation [Original Research].  
970 *Frontiers in Microbiology*, 8. <https://doi.org/10.3389/fmicb.2017.02003>
- 971